The Astrophysical Journal, 549, in press
Preprint typeset using LaTeX style emulateapj v. 04/03/99

WHERE IS THE [O III]λ4363 EMITTING REGION IN ACTIVE GALACTIC NUCLEI?

Tohru NAGAO[1], Takashi MURAYAMA[1], and Yoshiaki TANIGUCHI[1,2]
[1] Astronomical Institute, Graduate School of Science, Tohoku University, Aramaki, Aoba, Sendai 980-8578, Japan
[2] Institute for Astronomy, University of Hawaii, 2680 Woodlawn Drive, Honolulu, HI 96822

The Astrophysical Journal, 549, in press

ABSTRACT

The emission-line flux ratio of [O III]λ4363/[O III]λ5007 ($R_{\rm OIII}$) is a useful diagnostic for the ionization mechanism and physical properties of emission-line regions in active galactic nuclei (AGNs). However, it is known that simple photoionization models underpredict the [O III]λ4363 intensity, being inconsistent with observations. In this paper, we report on several pieces of evidence that a large fraction of the [O III]λ4363 emission arises from the dense gas obscured by putative tori: (1) the visibility of high-$R_{\rm OIII}$ regions is correlated to that of broad-line regions, (2) higher-$R_{\rm OIII}$ objects show hotter mid-infrared colors, (3) higher-$R_{\rm OIII}$ objects show stronger highly-ionized emission lines such as [Fe VII]λ6087 and [Fe X]λ6374, and (4) higher-$R_{\rm OIII}$ objects have broader line width of [O III]λ4363 normalized by that of [O III]λ5007. To estimate how such a dense component contributes to the total emission-line flux, dual-component photoionization model calculations are performed. It is shown that the observed values of $R_{\rm OIII}$ of type 1 AGNs may be explained by introducing a 5% – 20% contribution from the dense component while those of type 2 AGNs may be explained by introducing a 0% – 2% contribution. We also discuss the [O III]λ4363 emitting regions in LINERs in the framework of our dual-component model.

Subject headings: galaxies: nuclei - galaxies: Seyfert - quasars: emission lines

1. INTRODUCTION

It has been often considered that emission-line regions around active galactic nuclei (AGNs) are photoionized by the nonthermal continuum radiation from central engines (e.g., Davidson 1977; Yee 1980; Kwan & Krolik 1981; Shuder 1981; Cohen 1983; Cruz-González et al. 1991; Osterbrock 1993; Evans et al. 1999). However, this photoionization scenario has sometimes been confronted with several serious problems.

One of such problems is that any single-zone photoionization models underpredict the [O III]λ4363/[O III]λ5007 intensity ratio, $R_{\rm OIII}$ (e.g., Koski & Osterbrock 1976; Ferland & Netzer 1983; Filippenko & Halpern 1984; Viegas-Aldrovandi & Gruenwald 1988). The reason for the underprediction of $R_{\rm OIII}$ is thought to be that photoionization of gas in optically thick condition is hard to accomplish electron temperatures above a few $\times 10^4$ K if density of the gas is typical in narrow-line regions (NLRs). In order to solve this problem, many studies have been carried out. Such attempts can be roughly divided into the following two categories. One is based on the idea that a high density component may contribute to achieve the observed high $R_{\rm OIII}$ (e.g., Baldwin 1975; Osterbrock, Koski, & Phillips 1976; Filippenko & Halpern 1984; Filippenko 1985). This idea is attributed to the fact that the critical density ($n_{\rm cr}$) of the [O III]λ4363 emission (3.3×10^7 cm^{-3}) is higher than that of the [O III]λ5007 emission (7.0×10^5 cm^{-3}); which leads to high $R_{\rm OIII}$ when the gas density is higher than $\sim 10^6$ cm^{-3}. The other idea is to introduce high temperature regions whose temperature is more than a few times 10^4 K. To achieve such high temperatures, either shock-heated regions (e.g., Koski & Osterbrock 1976; Heckman 1980; Dopita & Sutherland 1995) or optically-thin components (e.g., Wilson, Binette, & Storchi-Bergmann 1997) is required.

In addition, some previous studies reported that the values of $R_{\rm OIII}$ depend on the AGN type; i.e., type 1 Seyfert nuclei (S1s) exhibit higher $R_{\rm OIII}$ than type 2 Seyfert nuclei (S2s) (e.g., Osterbrock et al. 1976; Heckman & Balick 1979; Shuder & Osterbrock 1981; Cohen 1983). This tendency seems to suggest that a part of the [O III]λ4363 emission arises from the regions which are obscured only in S2s by any materials, such as dusty tori. However, this tendency may be interpreted by the intrinsic (that is, not due to obscuration effects) difference of NLR properties, such as the size (Schmitt & Kinney 1996; Kraemer et al. 1998) or the ionization states (Schmitt 1998).

To investigate the reason why S1s show high $R_{\rm OIII}$ than S2s seems useful to explore where and how the [O III]λ4363 emission is radiated. Moreover, these may lead to the new solution to the underprediction problem of $R_{\rm OIII}$. Therefore, in this paper, we present how the observed values of $R_{\rm OIII}$ are different among various types of Seyferts based on a large sample of Seyferts compiled from the literature. Then, we compare $R_{\rm OIII}$ with various parameters and discuss the nature of the [O III]λ4363 emitting regions in AGNs.

2. DATA COMPILATION

2.1. *Data*

We briefly summarize the policy of classification of Seyfert nuclei in this paper, which is the same as that in Nagao, Taniguchi, & Murayama (2000c). Seyfert nuclei are often divided into three types based on the visibility of broad components of hydrogen recombination lines: i.e., S1, Seyfert 1.5 (S1.5), and S2. The S1s consist of typical

S1s (BLS1s; broad-line Seyfert 1 galaxies) and narrow-line Seyfert 1 galaxies (NLS1s; e.g., Osterbrock & Pogge 1985; Boller, Brandt, & Fink 1996). The type of Seyfert 1.2 (S1.2) is included in the type of BLS1 in this paper. We divide the type of S2 into $S2^+$ and $S2^-$; the former one exhibits the evidence for the existence of broad-line regions (BLRs) and the latter does not show such the evidence. For the convenience, both types of $S2^+$ and $S2^-$ are referred as $S2_{\rm total}$ when needed; i.e., $S2_{\rm total} = S2^+ + S2^-$. There are two populations in the types of $S2^+$: one shows weak symptoms of the existence of BLRs in their optical or near-infrared (NIR) spectra ($S2_{\rm RBLR}$; type 2 Seyfert with the reddened BLR) and another one exhibits the hidden BLR which is detected only in polarized spectra ($S2_{\rm HBLR}$). The type of $S2_{\rm RBLR}$ consists of Seyfert 1.8 galaxies (S1.8s), Seyfert 1.9 galaxies (S1.9s), and the Seyfert galaxies with the broad Paschen or Bracket line ($S2_{\rm NIR-BLR}$s). They are combined into $S2^+$ when statistical treatments are needed.

In order to investigate statistical properties of the observed values of $R_{\rm OIII}$ for each type of Seyferts, we compiled $R_{\rm OIII}$ from the literature. The number of compiled objects is 214; 26 NLS1s, 56 BLS1s, 54 S1.5s, 4 S1.8s, 16 S1.9s, 5 $S2_{\rm NIR-BLR}$s, 8 $S2_{\rm HBLR}$s, and 45 $S2^-$s. We basically referred to Véron-Cetty & Véron (1998) for the AGN type of each object. Though Mrk 335, Mrk 766, Mrk 1126, H 34.06, H 1934–063, HE 1029–1831, and J 13.12 are not classified as NLS1 by Véron-Cetty & Véron (1998), they are treated as NLS1 in this paper because they have been classified as NLS1 (Osterbrock & Pogge 1985; Vaughan et al. 1999; Rodríguez-Ardia, Pastoriza, & Donzelli 2000).

All the objects are listed in Table 1 together with their redshifts, $R_{\rm OIII}$, and the fluxes at 3.5μm, 12μm, 25μm, and 60μm. The values of $R_{\rm OIII}$ in this table are the averaged ones among the references given there. We do not make the reddening correction for the values of $R_{\rm OIII}$ since it is often difficult to measure the narrow Balmer component, particularly for S1s. It is noted that we do not use any upper limit data in this study.

2.2. *Selection Bias*

Because we do not impose any selection criteria upon our sample, it is necessary to test whether or not the various samples are appropriate for our comparative study. There would be possible biases if there are any systematic differences in the redshift distributions or in the intrinsic nuclear luminosity distributions, thus we investigate those distributions below.

First we investigate the redshift distributions. We show the histograms of redshift in Figure 1. The mean redshift and the 1σ deviation for each type are given in Table 2. There seems to be a tendency that the redshifts of the objects in the samples of the BLS1 and the S1.5 are larger than those in the other samples. In order to confirm whether or not this tendency is statistically real, we apply the Kolmogorov-Smirnov (KS) statistical test (see Press et al. 1988). The null hypothesis is that the redshift distributions among the NLS1s, the BLS1s, the S1.5s, the $S2^+$s, and the $S2^-$s come from the same underlying population. The KS probabilities are given in Table 3. The KS test leads to the following results. (1) The redsifts of the NLS1s, of the BLS1s, and of the S1.5s are statistically indistinguishable. (2) The redshifts of the $S2^+$ and of the $S2^-$ are also statistically indistinguishable. (3) However, the former and the latter are statistically different. Does this difference of the redshift cause any possible biases against the following comparative study? To investigate this issue, we examine the relation between $R_{\rm OIII}$, which is our main interest in this paper, and redshift (Figure 2). Figure 2 suggests that there is no correlation between $R_{\rm OIII}$ and redshift. This means that the redshift difference among the samples is thought not to cause a bias against the investigation of properties of $R_{\rm OIII}$.

Second we consider the intrinsic AGN power. The so-called AGN unified model (Antonucci & Miller 1985; see for a review Antonucci 1993) requires anisotropic nuclear radiation. This may cause systematic differences in intrinsic AGN power among the types of Seyferts depending on selection criteria. Statistical properties of emission-line ratios for each type of Seyferts might suffer from this bias of intrinsic luminosity. Therefore, we investigate the intrinsic AGN power distributions using the *IRAS* 60μm luminosity, which is regarded as rather isotropic emission (e.g., Pier & Krolik 1992; Efstathiou & Rowan-Robinson 1995; Fadda et al. 1998) though this might be contaminated with the influence of circumnuclear star formation. The histograms of the 60μm luminosity are shown in Figure 3. The mean 60μm luminosities and 1σ deviations are given in Table 2. Here we adopt a Hubble constant $H_0 = 50$ km s^{-1} Mpc^{-1} and a deceleration parameter $q_0 = 0$. We apply the KS test where the null hypothesis is that the distribution of the 60μm luminosity of the samples come from the same underlying population. The resultant KS probabilities are given in Table 3. The KS test suggests that there is no systematic difference in the 60μm luminosity among the types of Seyfert galaxies. It is noted that there is no correlation between $R_{\rm OIII}$ and the 60μm luminosity, i.e., the intrinsic AGN power (Figure 4).

3. RESULTS

3.1. *Dependence of $R_{\rm OIII}$ on the AGN Type*

We show the histograms of $R_{\rm OIII}$ for each type of Seyfert galaxies in Figure 5. The mean and the 1σ deviation of $R_{\rm OIII}$ for each type are given in Table 2. In Figure 5, it is clearly shown that the $S2_{\rm total}$s exhibit lower $R_{\rm OIII}$ than the NLS1s, the BLS1s, and the S1.5s. There seems to be a tendency also in details of the $S2_{\rm total}$s; i.e., the values of $R_{\rm OIII}$ of the S1.8s are higher than those of the S1.9s, and those of the S1.9s are higher than those of the $S2_{\rm NIR-BLR}$s, the $S2_{\rm HBLR}$s, and the $S2^-$s although the numbers of the samples are small. These properties can be interpreted that the more the BLR emission suffers the reddening, the lower the observed value of $R_{\rm OIII}$ is. We apply the KS test where the null hypothesis is that the distribution of $R_{\rm OIII}$ of the various types comes from the same underlying population. The resultant KS probabilities are given in Table 3. The KS test leads to the following results. (1) The NLS1s, the BLS1s, and the S1.5s are statistically indistinguishable in the frequency distribution of $R_{\rm OIII}$. (2) The $S2^+$ and the $S2^-$ are also statistically indistinguishable. (3) However, the NLS1s, of the BLS1s, and of the S1.5s have statistically higher $R_{\rm OIII}$ values than the $S2^+$s and the $S2^-$s. These results are consistent with the previous works; Osterbrock et al. (1976), Heckman & Balick (1979), and Shuder & Osterbrock (1981) have mentioned that the S1s show higher $R_{\rm OIII}$ values than the S2s, and

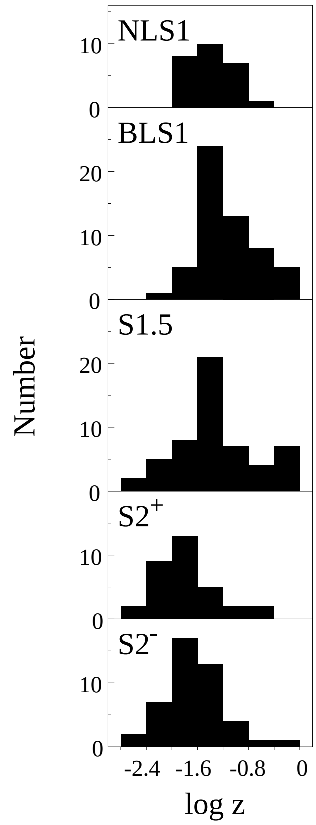

FIG. 1.— The frequency distributions of the redshift for the NLS1s, the BLS1s, the S1.5s, the $S2^{+}$s, and the $S2^{-}$s.

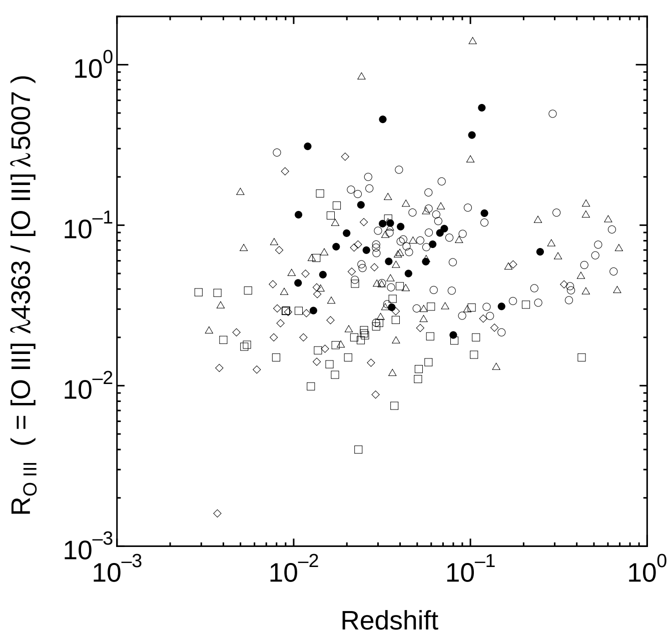

FIG. 2.— $R_{\rm OIII}$ are plotted as a function of the redshift. The NLS1s, the BLS1s, the S1.5s, the $S2^{+}$s, and the $S2^{-}$s are shown by filled circles, open ones, triangles, diamonds, and squares, respectively.

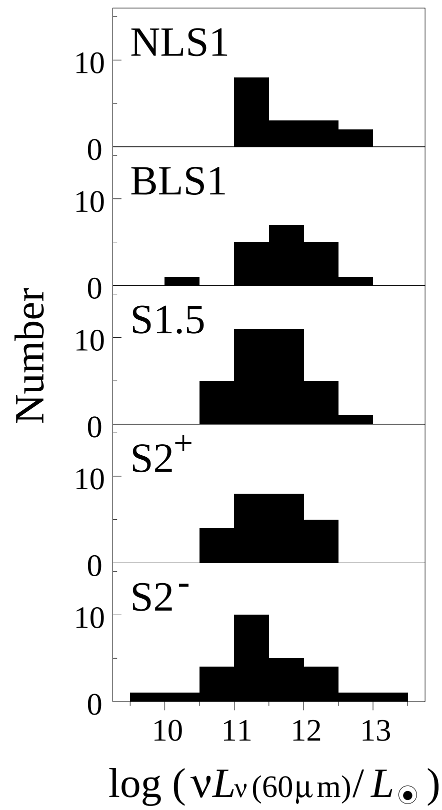

FIG. 3.— The frequency distributions of the 60μm luminosity for the NLS1s, the BLS1s, the S1.5s, the S2^{+}s, and the S2^{-}s. The luminosities are normalized by the solar luminosity.

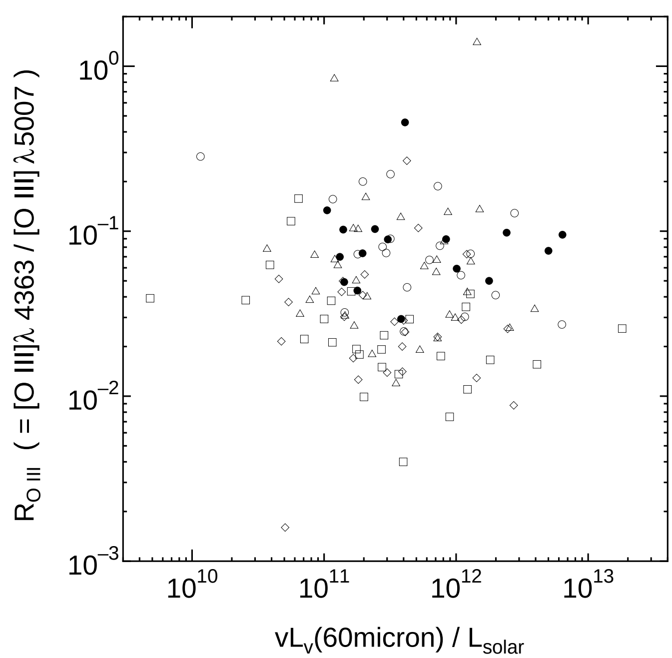

FIG. 4.— $R_{\rm OIII}$ are plotted as a function of the 60μm luminosity. The symbols are the same as in Figure 2.

Table 2

Means and Deviations of Redshift, $\nu L_\nu(60\mu)$, and $R_{\rm OIII}$ for Each Types of Seyfert Galaxies

type[a]	Redshift	log ($\nu L_\nu(60\mu{\rm m})/L_\odot$)	$R_{\rm OIII}$
NLS1 (26)	0.0567 ± 0.0532	11.694 ± 0.563	0.126 ± 0.132
BLS1 (56)	0.1329 ± 0.1612	11.664 ± 0.571	0.091 ± 0.077
S1.5 (54)	0.1192 ± 0.1768	11.546 ± 0.499	0.107 ± 0.210
$S2_{\rm total}$ (78)	0.0407 ± 0.0674	11.454 ± 0.621	0.039 ± 0.044
$S2^+$ (33)	0.0375 ± 0.0657	11.480 ± 0.496	0.047 ± 0.054
S1.8 (4)	0.0996 ± 0.1383	11.694 ± 0.387	0.097 ± 0.070
S1.9 (16)	0.0255 ± 0.0401	11.368 ± 0.495	0.053 ± 0.060
$S2_{\rm NIR-BLR}$ (5)	0.0594 ± 0.0564	11.368 ± 0.109	0.029 ± 0.021
$S2_{\rm HBLR}$ (8)	0.0168 ± 0.0104	11.635 ± 0.522	0.023 ± 0.011
$S2^-$ (45)	0.0431 ± 0.0685	11.429 ± 0.717	0.033 ± 0.032

[a]The number of objects for each type is written in parenthesis.

Table 3

The Results of the KS Test Concerning the Redshift, $\nu L_\nu(60\mu)$, and $R_{\rm OIII}$.

Type	NLS1	BLS1	S1.5	$S2^+$	$S2^-$
			Redshift		
NLS1	⋯	1.671×10^{-1}	6.734×10^{-1}	1.831×10^{-3}	8.579×10^{-2}
BLS1	⋯	⋯	6.818×10^{-2}	3.525×10^{-9}	5.410×10^{-6}
S1.5	⋯	⋯	⋯	5.872×10^{-6}	3.685×10^{-3}
$S2^+$	⋯	⋯	⋯	⋯	1.624×10^{-1}
$S2^-$	⋯	⋯	⋯	⋯	⋯
			$\nu L_\nu(60\mu{\rm m})$		
NLS1	⋯	8.792×10^{-1}	7.908×10^{-1}	8.970×10^{-1}	3.923×10^{-1}
BLS1	⋯	⋯	4.439×10^{-1}	5.986×10^{-1}	1.920×10^{-1}
S1.5	⋯	⋯	⋯	4.788×10^{-1}	6.648×10^{-1}
$S2^+$	⋯	⋯	⋯	⋯	7.911×10^{-1}
$S2^-$	⋯	⋯	⋯	⋯	⋯
			$R_{\rm OIII}$		
NLS1	⋯	7.877×10^{-1}	2.037×10^{-1}	1.555×10^{-4}	9.933×10^{-9}
BLS1	⋯	⋯	4.064×10^{-1}	5.735×10^{-5}	4.612×10^{-10}
S1.5	⋯	⋯	⋯	2.045×10^{-3}	4.106×10^{-6}
$S2^+$	⋯	⋯	⋯	⋯	1.264×10^{-1}
$S2^-$	⋯	⋯	⋯	⋯	⋯

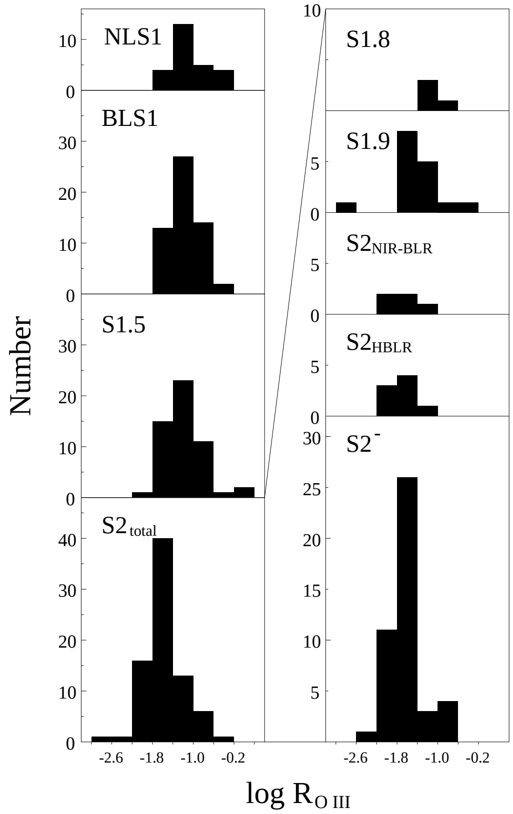

FIG. 5.— The frequency distributions of $R_{\rm OIII}$ for the NLS1s, the BLS1s, the S1.5s, and the $\rm S2_{total}$s. The details of the frequency distributions of the $\rm S2_{total}$s are also shown: i.e., for the S1.8s, the S1.9s, the $\rm S2_{NIR-BLR}$s, the $\rm S2_{HBLR}$s, and the $\rm S2^{-}$s.

Cohen (1983) has found that the S1.5s also show higher $R_{\rm OIII}$ values than the S2s. Nagao, Murayama, & Taniguchi (2000a) recently confirmed that the observed $R_{\rm OIII}$ values are statistically indistinguishable between the NLS1s and the BLS1s (see also Rodríguez-Ardia et al. 2000).

It seems possible that the difference in $R_{\rm OIII}$ among the types of Seyfert galaxies is attributed to the systematic difference in the amounts of the reddening, because we do not make any reddening correction for the compiled emission-line flux data. Thus we investigate the reddening effect on $R_{\rm OIII}$ adopting the Cardelli's extinction curve (Cardelli, Clayton, & Mathis 1989). It results in that the correction factors for the observed value of $R_{\rm OIII}$ is 1.222 for the reddening if we assume $A_V = 1.0$ mag, which is typical difference in the amounts of reddening for NLRs between S1s and S2s (Dahari & De Robertis 1988; see also De Zotti & Gaskell 1985). This factor is too small to explain the systematic difference of $R_{\rm OIII}$ among the types of Seyfert galaxies. Therefore we conclude that the reason of the systematic difference of $R_{\rm OIII}$ among the Seyfert types is not the extinction effect but any other mechanism, discussed later.

3.2. *Correlation between $R_{\rm OIII}$ and MIR-Color*

Dust grains within dusty tori in AGNs absorb NIR to soft X-ray photons emitted from the central engine, and re-emit the thermal radiation in the mid-infrared (MIR) regime. Since the tori are quite optically thick, the MIR spectrum has strong dependence on the viewing angle (e.g., Heckman, Chanbers, & Postman 1992; Giuricin, Mardirossian, & Mezzetti 1995; Heckman 1995; Fadda et al. 1998; Murayama, Mouri & Taniguchi 2000). This means that the hot inner surface of dusty tori is seen when the torus is observed from a favored (i.e., more face-on) view but obscured when observed from a unfavored (i.e., more edge-on) view. Therefore, it is interesting to investigate correlations between the MIR colors and $R_{\rm OIII}$.

The dependences of $R_{\rm OIII}$ on the flux ratios of *IRAS* 12 μm and L band to *IRAS* 25 μm are shown in Figure 6. These two flux ratios are used to investigate the visibility of the hot inner surface of dusty tori in AGNs. The method using the flux ratio of L band to *IRAS* 25 μm is proposed by Murayama et al. (2000) for the purpose of reducing the influence of star-formation. In Figure 6, there appears a positive correlation in each diagram. In order to investigate whether or not these positive correlations are statistically significant, we apply the Spearman's rank test (see Press et al. 1988) where the null hypothesis is that the observed value of $R_{\rm OIII}$ is not correlated with the flux ratios of *IRAS* 12 μm and of L band to *IRAS* 25 μm. The resulting probabilities are 3.598 $\times 10^{-5}$ for the flux ratio of *IRAS* 12 μm to *IRAS* 25 μm and 3.254 $\times 10^{-4}$ for the flux ratio of L band to *IRAS* 25 μm, which mean that the positive correlations shown in Figure 6 are statistically real. This means that the hotter the observed MIR colors are, the higher the observed values of $R_{\rm OIII}$ are.

3.3. *Correlation between $R_{\rm OIII}$ and HINER Components*

Pier & Voit (1995) investigated the hydrodynamic and line-emitting properties of dense clouds exposed to an AGN continuum emission at the inner edge of the torus. Since such regions have a large covering factor and a high

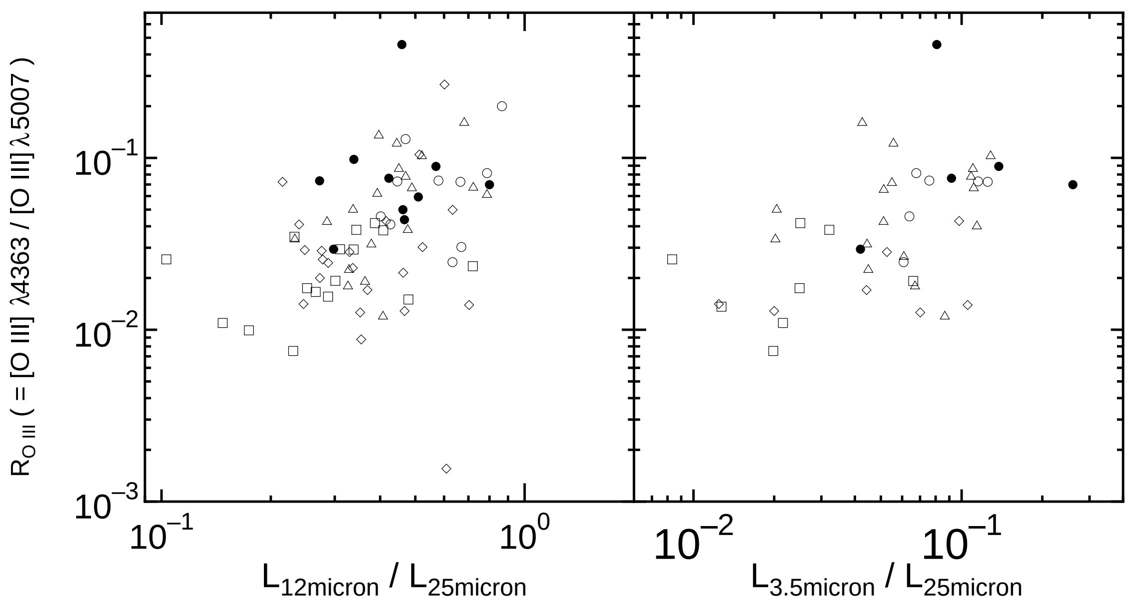

FIG. 6.— $R_{\rm OIII}$ are plotted as functions of the flux ratios of *IRAS* 12 μm (left) and of *L*-band (right) to *IRAS* 25 μm. The symbols are the same as in Figure 2.

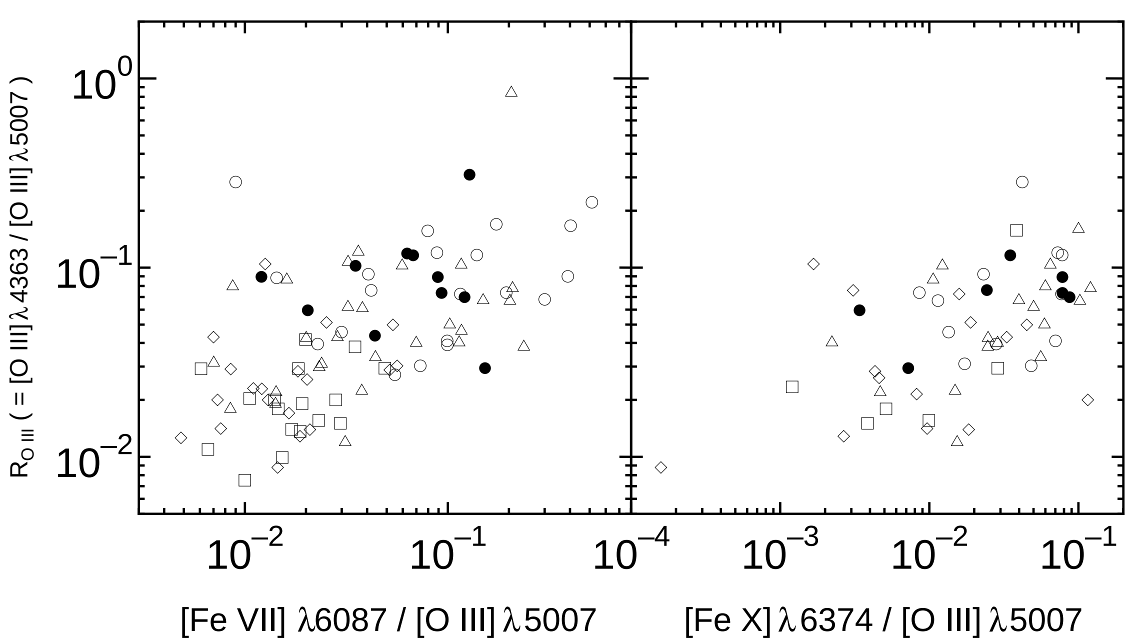

FIG. 7.— $R_{\rm OIII}$ are plotted as functions of the line ratios of [Fe VII]λ6087/[O III]λ5007 (left) and of [Fe X]λ6374/[O III]λ5007 (right). The symbols are the same as in Figure 2.

density ($n_{\rm H} \sim 10^{7-8}$ cm^{-3}), those clouds are thought to be a plausible place to produce the highly-ionized emission lines such as [Fe VII]λ6087 and [Fe X]λ6374[1]. This picture is consistent with the fact that such highly-ionized emission lines are stronger in S1s than in S2s (Murayama & Taniguchi 1998a; Nagao et al. 2000c). That is, a large part of the high-ionization nuclear emission-line regions (HINERs; Binette 1985; Murayama, Taniguchi, & Iwasawa 1998) is located at the region which is obscured in S2s by any materials, such as dusty tori.

Since $R_{\rm OIII}$ is higher in S1s than in S2s and $n_{\rm cr}$ of the [O III]λ4363 emission is comparable with $n_{\rm cr}$ of [Fe VII]λ6087, it is interesting to investigate the relation between the intensity of the [O III]λ4363 emission and those of the HINER emission lines, [Fe VII]λ6087 and [Fe X]λ6374. The flux of these HINER lines is normalized by the flux of [O III]λ5007 following the manner of Murayama & Taniguchi (1998a) and Nagao et al. (2000c). The results are shown in Figure 7. There is a positive correlation for each case, especially between $R_{\rm OIII}$ and the flux ratio of [Fe VII]λ6087/[O III]λ5007. This means that the strong [O III]λ4363 emitting regions are located at the same place as the HINERs.

It should be noted that the value of $R_{\rm OIII}$ correlates to the intensity of [Fe X]λ6374 worse than to that of [Fe VII]λ6087. This is consistent with the remark of Nagao et al. (2000c) that the intensity of [Fe X]λ6374 is less suitable to investigate the viewing angle toward tori than that of [Fe VII]λ6087; they claimed that a part of the [Fe X]λ6374 emission is radiated from spatially extended, low-density gas (see also Korista & Ferland 1989; Golev et al. 1995; Murayama et al. 1998; Nagao et al. 2000b).

3.4. *Kinematical Investigation of [O III] Emitting Regions*

Emission-line width of the NLR emission gives us some pieces of useful information about the kinematical and geometrical properties of gas clouds in the NLRs. Some earlier works have shown that there is a correlation between the emission-line width and $n_{\rm cr}$ of the emission line [e.g., Pelat, Fosbury, & Alloin 1981; Atwood, Baldwin, & Carswell 1982; Filippenko & Halpern 1984; De Robertis & Osterbrock 1984 (DRO84); Filippenko 1985; De Robertis & Osterbrock 1986 (DRO86); Appenzeller & Östreicher 1988; Espey et al. 1994]. This correlation is broadly interpreted as follows. A given emission line is emitted most efficiently from gas clouds whose densities are close to $n_{\rm cr}$. On the other hand, we can use line width as a rough measure of location of the emitting region if we assume that the NLR line widths are dominated either by random virialized motion or by Keplerian rotation. Therefore the correlation between line width and $n_{\rm cr}$ suggests that high-density gas clouds are located near the central engine relative to low-density gas clouds (DRO84; DRO86; see also Ferguson et al. 1997). This allows us to study the geometrical relationship between the [O III]λ4363 and the [O III]λ5007 emitting regions.

DRO84 measured the line widths of [O III]λ4363 and [O III]λ5007 for 11 broad-line Seyfert galaxies (NLS1s, BLS1s, and S1.5s) and DRO86 measured those for 13 narrow-line Seyfert galaxies (S2$^+$s and S2$^-$s). Using these data, which are corrected for the instrumental broadening, we compare the kinematical and geometrical properties between the [O III]λ4363 and the [O III]λ5007 emitting regions in the two samples. Note that the [O III]λ4363 emission is weak and that sometimes the deblending this line from Hγ may be difficult. Therefore we do not attempt to collect the line-width data from a large number of the literature and use only ones presented by De Robertis & Osterbrock. However, the difficulty in the measurement of the line widths may cause any systematical errors, which must be kept in mind. Since the numbers of the samples of DRO84 and DRO86 are small, we do not divide the sample into more detailed ones in this section.

The means and the 1σ deviations of the full-width at half maximum (FWHM) of [O III]λ4363 and [O III]λ5007, and ratios of them are given in Table 4. The histograms of these parameters are shown in Figure 8. In order to investigate whether or not the distributions of the line width of [O III]λ4363 and that of [O III]λ5007 are statistically different, and whether or not these distributions are statistically different between the samples of DRO84 and DRO86, we apply the KS test. The KS test leads to the following results. (1) For the DRO84 sample, FWHM([O III]λ4363) is larger than FWHM([O III]λ5007) though the statistical significance is low ($P_{\rm KS}$ = 0.012). (2) For the DRO86 sample, FWHM([O III]λ4363) and FWHM([O III]λ5007) are statistically indistinguishable ($P_{\rm KS} = 0.226$). (3) FWHM([O III]λ4363) of the DRO84 sample is larger than that of the DRO86 sample though the statistical significance is low ($P_{\rm KS} = 0.023$). (4) FWHM([O III]λ5007) of the DRO84 sample and that of the DRO86 sample are statistically indistinguishable ($P_{\rm KS} = 0.330$). And finally, (5) the ratio of FWHM([O III]λ4363)/FWHM([O III]λ5007) of the DRO84 sample is larger than that of the DRO86 sample though the statistical significance is low ($P_{\rm KS}$ = 0.023). These results are summarized in Table 5. All these results support the idea that the strong [O III]λ4363 emitting region is located at inner region comparing to the [O III]λ5007 emitting region, and such a strong [O III]λ4363 emitting region is visible only in S1s but obscured in S2s, although a much larger sample will be necessary to confirm these arguments.

To investigate the relationship between the visibility and kinematics of the [O III]λ4363 emitting regions more directly, we examine the dependence of $R_{\rm OIII}$ on FWHM([O III]λ4363) and that on the ratio of FWHM([O III]λ4363)/FWHM([O III]λ5007) in Figure 9. In order to examine whether or not there are any correlations in these parameters statistically, we apply the Spearman's rank test where the null hypothesis is that the observed value of $R_{\rm OIII}$ is not correlated with FWHM([O III]λ4363) or FWHM([O III]λ4363)/FWHM([O III]λ5007). The resulting probabilities are 0.165 for FWHM([O III]λ4363) and 0.032 for FWHM([O III]λ4363)/FWHM([O III]λ5007). These results mean that there is no correlation between $R_{\rm OIII}$ and FWHM([O III]λ4363) while there is a marginal tendency of a positive correlation between $R_{\rm OIII}$ and the ratio of FWHM([O III]λ4363)/FWHM([O III]λ5007). This

[1]The critical densities of these emission lines are 3.6 $\times 10^7$ cm^{-3} for [Fe VII]λ6087 and 4.8 $\times 10^9$ cm^{-3} for [Fe X]λ6374 (De Robertis & Osterbrock 1986b). Thus these highly ionized emission lines can be radiated in the clouds of $n_{\rm H} \sim 10^{7-8}$ cm^{-3}. However, low-ionization emission lines such as [O III]λ5007 are suppressed by a collisional de-excitation in such a dense gas cloud because $n_{\rm cr}$ of low-ionization emission lines are generally low comparing to $n_{\rm H}$ of the dense gas clouds.

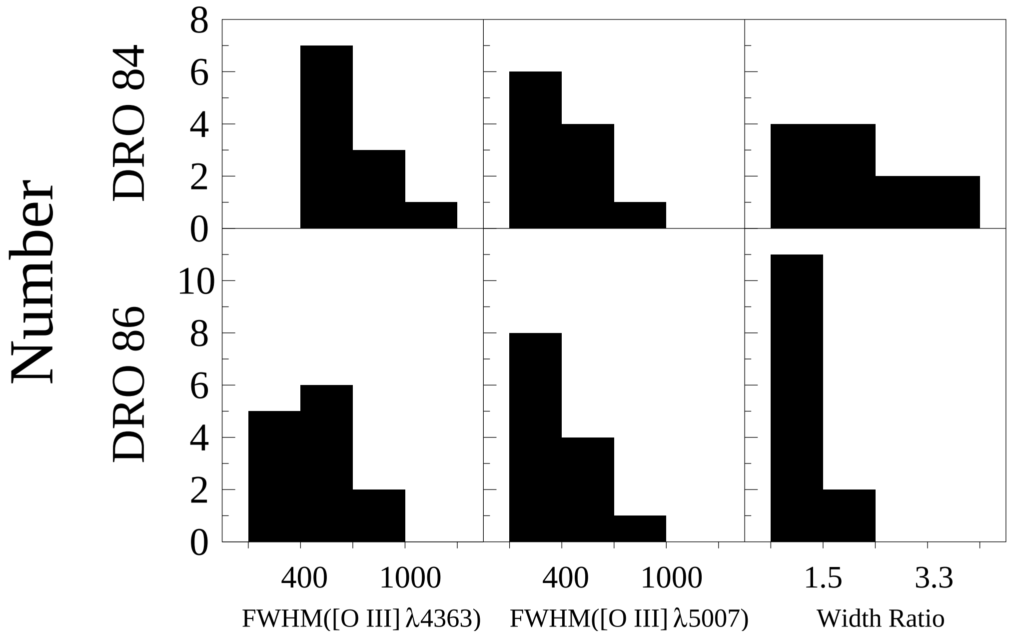

FIG. 8.— The frequency distributions of FWHM([O III]λ4363) (left), FWHM([O III]λ5007) (middle), and the ratio of FWHM([O III]λ4363) to FWHM([O III]λ5007) (right) for the samples of DRO84, which represent broad-line Seyfert galaxies (upper), and of DRO86, which represent narrow-line Seyfert galaxies (lower).

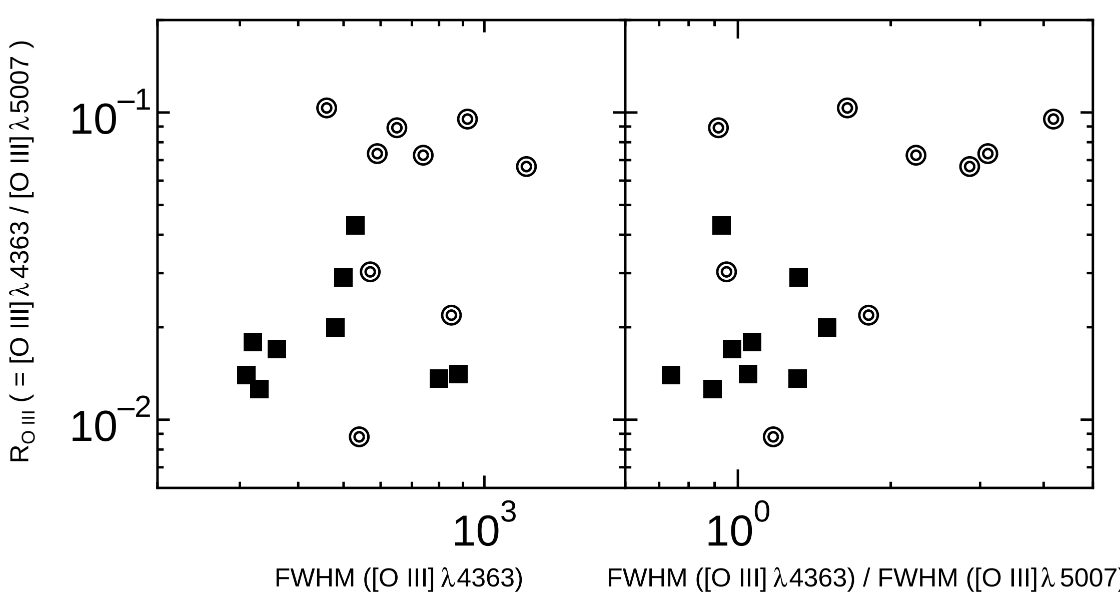

FIG. 9.— $R_{\rm OIII}$ are plotted as functions of FWHM([O III]λ4363) (left) and the ratio of FWHM([O III]λ4363) to FWHM([O III]λ5007) (right). The objects in DRO84 sample and in DRO86 are shown by circles and filled squares, respectively.

Table 4
The Statistical Properties for the Sample of DRO84[a] and DRO86[b]

sample		mean and deviation
DRO84	FWHM([O III]λ4363)	684 ± 225
	FWHM([O III]λ5007)	387 ± 157
	FWHM([O III]λ4363)/FWHM([O III]λ5007)	2.03 ± 0.96
DRO86	FWHM([O III]λ4363)	492 ± 168
	FWHM([O III]λ5007)	434 ± 147
	FWHM([O III]λ4363)/FWHM([O III]λ5007)	1.16 ± 0.25

[a]De Robertis & Osterbrock (1984).

[b]De Robertis & Osterbrock (1986).

Table 5
The Results of the KS Test Concerning the Kinematic Properties

	KS Prob.
FWHM([O III]λ4363) versus FWHM([O III]λ5007)	
DRO84	0.012
DRO86	0.226
DRO84 versus DRO86	
FWHM([O III]λ4363)	0.023
FWHM([O III]λ5007)	0.330
FWHM([O III]λ4363)/FWHM([O III]λ5007)	0.023

difference is caused because FWHM([O III]λ4363) reflects not only the location of the [O III]λ4363 emitting region but also the mass of a supermassive black hole while the effect of the dispersion of the mass of a supermassive black hole among objects is reduced in the value of FWHM([O III]λ4363)/FWHM([O III]λ5007).

It should be noted that there are some lines of evidence which show that some of broader emission-line widths of highly-ionized emission lines are due to outflows, not to the depth of gravitational potentials (e.g., Moore & Cohen 1996; Kaiser et al. 2000; Nelson et al. 2000; Crenshaw & Kraemer 2000). If this is the case, line widths might not contain the information concerning the geometry of line-emitting gas clouds. However, unfortunately, the present data cannot distinguish these two interpretations.

4. DISCUSSION

4.1. *Where is the [O III]λ4363 Emitting Region in AGNs?*

In this section, we discuss why the observed values of $R_{\rm OIII}$ are higher in S1s than in S2s and how the high $R_{\rm OIII}$ comparing to the predicted values by simple photoionization models is achieved.

The first problem is the type dependence of the observed values of $R_{\rm OIII}$, shown in Figure 5. There are two possible interpretations to understand this dependence. One is that the [O III]λ5007 emission is stronger in S2s than S1s due to the intrinsically (i.e., not due to inclination effects) larger size of NLRs of S2s as proposed by Schmitt & Kinney (1996). Another is that the strong [O III]λ4363 emitting regions exist somewhere but obscured by something on the line of sight when we see S2s. Because the intrinsic AGN luminosity is similar among the various types of Seyferts in our sample as mentioned in Section 2.2, the former case predicts the stronger [O III]λ5007 luminosity in S2s than in S1s and similar [O III]λ4363 luminosity among the Seyfert types. On the other hand, the latter case predicts the similar [O III]λ5007 luminosity among the Seyfert types and the stronger [O III]λ4363 luminosity in S1s than in S2s. These two cases may be the extreme ones and the real situation might be intermediate between the two cases. However, it is interesting to investigate which case is close to the observed properties of emission-line spectra. Therefore we compare the observed emission-line luminosity of [O III]λ5007 and [O III]λ4363 among various types of Seyferts, which is shown in Figure 10. To quantify the statistical significance of the difference in the luminosity distribution among the Seyfert types, we apply the KS test where the null hypothesis is that the distribution of these emission-line luminosities come from the same underlying population. The KS test leads to the following results. (1) The distributions of the [O III]λ5007 luminosity are statistically indistinguishable among the BLS1s, the S1.5s, and the S2s though the [O III]λ5007 luminosity of the NLS1s are weaker than that of other Seyfert types. (2) The distributions of the [O III]λ4363 luminosity are statistically indistinguishable among the NLS1s, BLS1s, and the S1.5s though the [O III]λ4363 luminosity of the S2s are weaker than that of the BLS1s and the S1.5s. The KS probabilities are given in Table 6. These results are consistent with the latter case; i.e., the type dependence of the observed values of $R_{\rm OIII}$ is not due to the dilution by a more extended NLR in S2s but due to the enhancement of the [O III]λ4363 emission in S1s. The reason why the [O III]λ5007 luminosity is smaller in the NLS1s than in other types may be that NLS1s are the extreme objects on the "eigenvector 1" of Boroson & Green (1992). More explicitly, there is a relation that the weaker the [O III]λ5007 emission is, the narrower the FWHM of Hβ is (e.g., Boroson & Green 1992; Brandt & Boller 1998; Sulentic et al. 2000). Following this relation, NLS1s may tend to exhibit weak [O III]λ5007 emissions as shown in Figure 10.

The properties of emission-line width described in Section 3.4 also support the idea that the dependence of $R_{\rm OIII}$ on AGN types is not due to the dilution of $R_{\rm OIII}$ by extended low density gas in S2s but due to the obscuration of the strong [O III]λ4363 emitting region in S2s. The S1s exhibit the broad [O III]λ4363 comparing to [O III]λ5007 while the S2s do not so. This suggests the existence of the inner, strong [O III]λ4363 emitting region which is obscured in S2s. We, therefore, conclude that the dependence of $R_{\rm OIII}$ on AGN types is attributed to the obscuration effect.

Now we consider the following problems. *Where is the [O III]λ4363 emitting region in AGNs?* And, *how is the high $R_{\rm OIII}$ comparing to the predicted values by simple photoionization models achieved?* According to the current unified model of AGNs, it is natural to consider that the material obscuring the strong [O III]λ4363 emitting regions in S2s is dusty tori. If this is the case, the strong [O III]λ4363 emitting region may be either the inner surface of dusty tori described by Pier & Voit (1995) or the dense gas clouds near the central engine, which are obscured by the tori, though these two alternatives cannot be distinguished only by the statistical tests presented in this paper. This is consistent with the similarity of the location between the HINER and the strong [O III]λ4363 emitting region, which is suggested by the correlation between the intensity of the HINER emission and $R_{\rm OIII}$ (see Section 3.3) because large parts of the HINER emission is thought to arise from such dense clouds (Pier & Voit 1995; Murayama & Taniguchi 1998a, 1998b; Nagao et al. 2000c). The MIR properties described in Section 3.2 also support this geometrical consideration of the [O III]λ4363 emitting region; i.e., the correlations between the MIR colors and $R_{\rm OIII}$ mean the similarity between the visibility of relatively hot inner surface of dusty tori and that of the strong [O III]λ4363 emitting region.

However, some of S2s also exhibit large $R_{\rm OIII}$, which is also difficult to be explained by the simple one-zone photoionization model. They may be have dense gas clouds in NLR, which is not obscured by dusty tori because of the large distance from the nucleus, or the escaping [O III]λ4363 emission from the leaky parts of the tori.

4.2. *Interpretation Using the Dual-Component Photoionization Model*

As described in Section 4.1, high-density gas clouds obscured by tori, which are located either at the inner surface of dusty tori or near the central engine where is obscured by the tori, are thought to emit a large fraction of the [O III]λ4363 emission. In order to investigate whether or not such an idea is consistent with photoionization scenarios quantitatively, we perform dual-component photoionization model calculations following the manner of Murayama

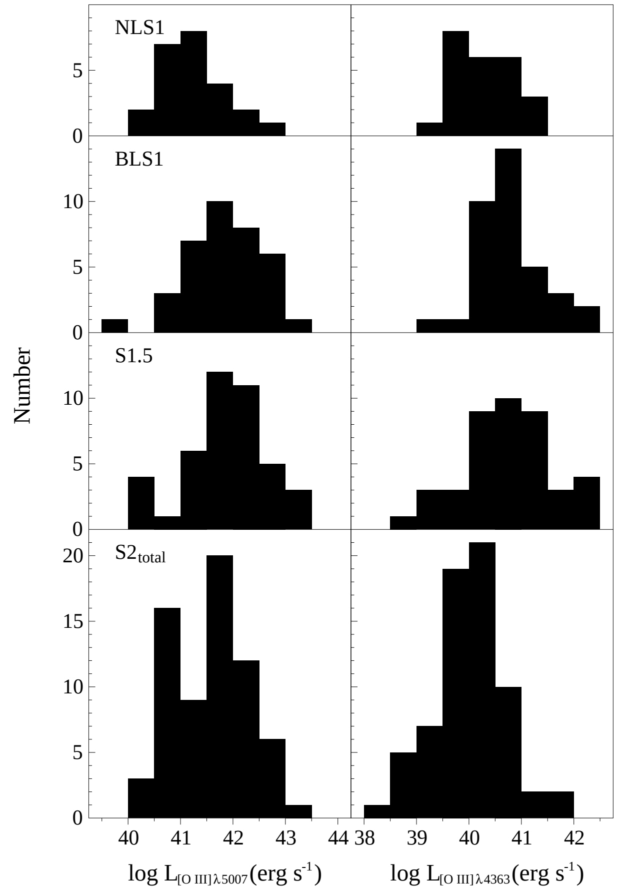

FIG. 10.— The frequency distributions of the [O III]λ5007 luminosity (left) and the [O III]λ4363 luminosity (right) for the NLS1s, the BLS1s, the S1.5s, and the $S2_{total}$s.

TABLE 6
THE RESULTS OF THE KS TEST CONCERNING THE $L_{[OIII]\lambda5007}$ AND $L_{[OIII]\lambda4363}$

Type	NLS1	BLS1	S1.5	$S2_{total}$
		$L_{[OIII]\lambda5007}$		
NLS1	···	4.291×10^{-3}	4.394×10^{-4}	4.445×10^{-2}
BLS1	···	···	9.312×10^{-1}	8.359×10^{-2}
S1.5	···	···	···	1.225×10^{-2}
$S2_{total}$	···	···	···	···
		$L_{[OIII]\lambda4363}$		
NLS1	···	2.519×10^{-2}	2.263×10^{-2}	4.419×10^{-1}
BLS1	···	···	7.925×10^{-1}	2.515×10^{-5}
S1.5	···	···	···	5.194×10^{-5}
$S2_{total}$	···	···	···	···

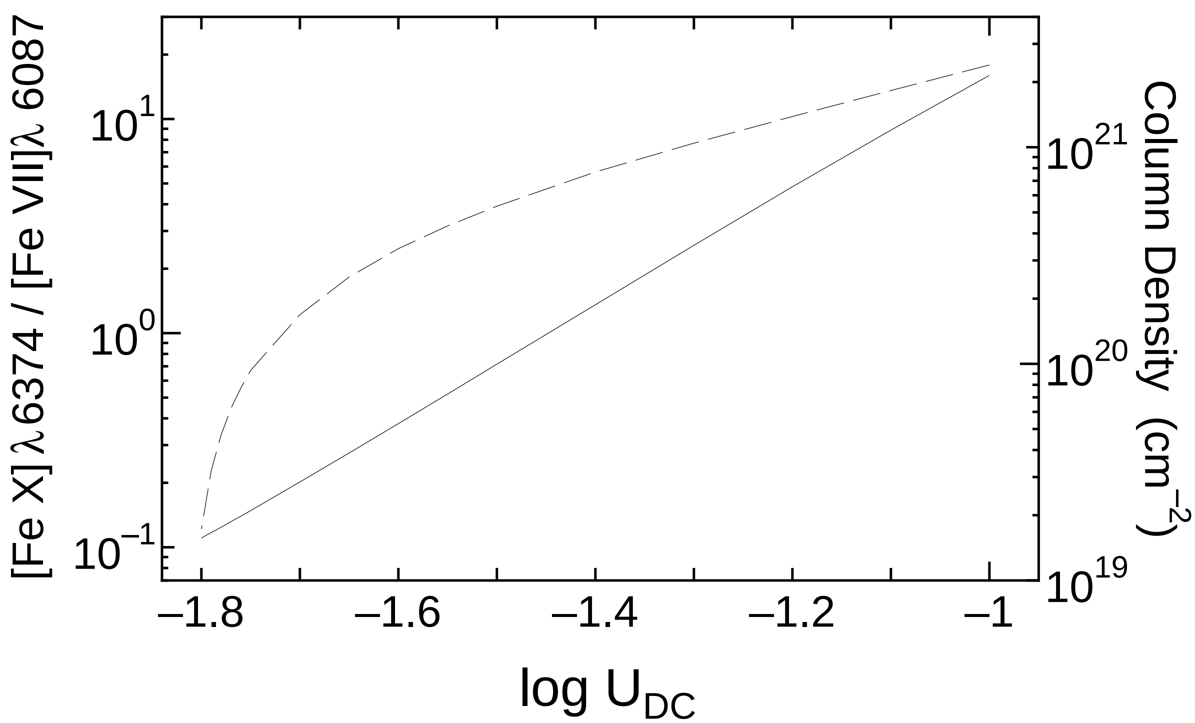

FIG. 11.— The calculated emission-line ratio of [Fe X]λ6374/[Fe VII]λ6087 (solid line) and the column density (dashed line) of the truncated torus component are shown as functions of the ionization parameter of the torus component, $U_{\rm DC}$.

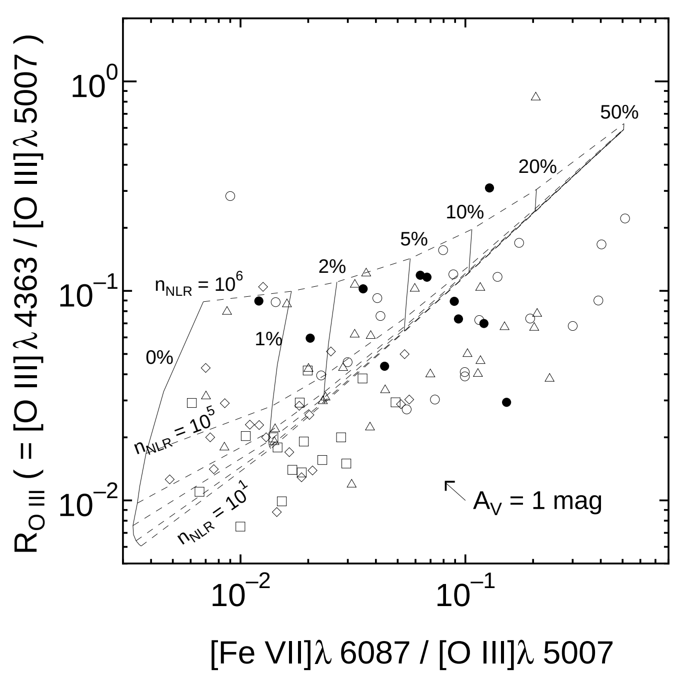

FIG. 12.— The diagram of $R_{\rm OIII}$ versus [Fe VII]λ4363/[O III]λ5007. The symbols are the same as in Figure 2. Our model calculations are superposed in the figure. The fraction of the contribution from torus components are also shown. The data points will move on the diagram as shown by the arrow if the extinction correlation of $A_V = 1.0$ is applied.

& Taniguchi (1998b). This method takes account of such high-density gas clouds as a strong [O III]λ4363 emitter, in addition to the typical NLR component. Here we assume the second situation, i.e., the strong [O III]λ4363 emitting region is not physically associated by the tori. Therefore we do not consider effects of dust, such as depletion of heavy metals, through the following calculations.

Our calculation methods are as follows. We perform photoionization model calculations using the spectral synthesis code *Cloudy* version 90.04 (Ferland 1996), which solves the equations of statistical and thermal equilibrium and produces a self-consistent model of the run of temperature as a function of depth into the nebula. Here we assume an uniform-density gas cloud with a plane-parallel geometry. The dense component (DC) is assumed to be truncated clouds; i.e., optically thin clouds for the ionizing photons, for the purpose of avoiding unusually strong [O I] emission (see Murayama & Taniguchi 1998b). The parameters for the calculations are (1) the hydrogen density of the cloud ($n_{\rm DC}$ and $n_{\rm NLR}$), (2) the ionization parameter ($U_{\rm DC}$ and $U_{\rm NLR}$), which is defined as the ratio of the ionizing photon density to the electron density, (3) the thickness of the torus component which is represented by the optical depth for ionizing photons, (4) the chemical compositions of the gas, (5) the shape of the input SED of ionizing photons, and (6) the fraction of DC to the NLR component.

Here we assume $n_{\rm DC} = 10^7$ cm^{-3}. We perform several model runs covering 10^1 cm$^{-3} \leq n_{\rm NLR} \leq 10^6$ cm^{-3}. The ionization parameter of the NLR component is assumed as $U_{\rm NLR} = 10^{-2}$. The ionization parameter and the hydrogen column density of DC are determined using following two conditions; ([Fe X]λ6374/[Fe VII]λ6087)$_{\rm DC}$ = 0.8 and ([Fe VII]λ6087/[O III]λ5007)$_{\rm DC}$ = 1.0. The former ratio is the typical value of Seyfert galaxies (Nagao et al. 2000c) and the latter condition is introduced by Murayama & Taniguchi (1998b) as a truncated dense gas cloud. As the result, $U_{\rm DC} = 10^{-1.48}$ and $N_{\rm DC} = 10^{20.76}$ cm^{-2} are adopted [2] (see Figure 10). The calculations are stopped when the gas temperature falls to 4000 K for the NLR component. We set the gas-phase elemental abundances to be solar ones taken from Grevesse & Anders (1989) with extensions by Grevesse & Noels (1993). We adopt the power-law continuum as the input spectrum, where the spectral index is assumed as $\alpha = -1.5$ (see Ferland & Netzer 1983) between 10 μm and 50 keV for the form $f_\nu \propto \nu^\alpha$. The spectral index is set to $\alpha = 2.5$ at lower energy (i.e., $\lambda \geq 10\mu$m) and to $\alpha = -2$ at higher energy (i.e., $h\nu \geq 50$ keV). The fraction of DC to the NLR component is treated as a free parameter in our calculations. The further details for this dual-component photoionization model are described in Murayama (1998) and Murayama & Taniguchi (1998b).

We present our results of model calculations and compare them with the observations in Figure 12, which is a diagram of $R_{\rm OIII}$ versus [Fe VII]λ6087/[O III]λ5007. We find that the model grids are roughly consistent with the observations if we take the effects of the correction for the extinction into account. Though the dispersion of observation is larger than the model grids, this is thought to be attributed the fact that the parameters, such as $U_{\rm DC}$, $U_{\rm NLR}$, $n_{\rm DC}$, and $N_{\rm DC}$, are different from object to object. It is shown that the $R_{\rm OIII}$ of the S1s can be explained by introducing a 5% $\sim$ 20% contribution from DC while the $R_{\rm OIII}$ of the S2s can be explained by introducing a 0% $\sim$ 2% contribution from DC. These fractions are consistent with the results of Murayama & Taniguchi (1998b), who introduce a $\sim$ 10% contribution from the dense gas clouds to explain intensities of the HINER emission of S1s.

4.3. $R_{\rm OIII}$ *in LINERs*

In some low-ionization nuclear emission-line regions (LINERs), the observed values of $R_{\rm OIII}$ are far larger than that predicted by one-zone photoionization models. Because of this property, the dominant mechanism for the ionization in LINERs has been frequently regarded as shock ionization (e.g., Fosbury et al. 1978; Heckman 1980; Baldwin, Phillips, & Terlevich 1981). However, Filippenko (1985) pointed out that there is a correlation between the emission-line width and $n_{\rm cr}$ of the emission line over the range 10^3 cm^{-3} $\leq n_{\rm cr} \leq 10^7$ cm^{-3} in a LINER PKS 1718-649. This suggests that LINERs may also possess high-density regions up to 10^7 cm^{-3}, which mean that the high $R_{\rm OIII}$ in LINERs may be explained by photoionization models.

Although it is not clear whether or not there is a dusty torus in all LINERs, there is several pieces of evidence that the unified models of AGNs can apply to some of LINERs; i.e., some LINERs exhibit broad components in their optical spectra (e.g., Ho et al. 1997b), in UV spectra (e.g., Barth et al. 1996), or only in polarized spectra (Barth, Filippenko, & Moran 1999a, 1999b). Therefore it is interesting to examine the properties of $R_{\rm OIII}$ of LINERs in the framework of our dual component model.

In order to investigate this issue, we compiled $R_{\rm OIII}$ of LINERs from the literature. Since the optical spectra of LINERs are often contaminated by stellar features from the host galaxy strongly, careful subtraction of such stellar features from observed spectra is needed to discuss the properties of faint emission lines such as [O III]λ4363. Our compiled sample consists of the objects that such careful subtraction was applied to; 8 LINERs with broad components (L1.9s) and 7 LINERs without broad components (L2s). Here it must be kept in mind that some of the L2s may not be AGNs; a part of LINERs may be shock-heated galaxy (e.g., Heckman 1980; Baldwin et al. 1981; Heckman 1986; Gonzárez Delgado & Pérez 1996) and others may be the objects ionized by hot stellar component (e.g., Filippenko & Terlevich 1992; Binette et al. 1994; Alonso-Herrero et al. 2000; Taniguchi, Shioya, & Murayama 2000). It is noted that the compiled samples may be biased in favor of the higher $R_{\rm OIII}$ objects because it is often difficult to detect weak [O III]λ4363 emission owing to the relatively strong stellar feature. The objects we compiled are given in Table 7, and the histograms of $R_{\rm OIII}$ for the L1.9s and the L2s are shown in Figure 13. The means and the deviations of $R_{\rm OIII}$ are 0.099 $\pm$ 0.054 for the L1.9s and 0.048 $\pm$ 0.030 for the L2s. There are a tendency that the values of the L1.9s are higher than those of L2s though these are statistically indistinguishable ($P_{\rm KS}$ = 0.252).

[2] Because it is known that there is uncertainty in collision strengths for the [Fe X]λ6374 emission, the derived values of $U_{\rm DC}$ and $N_{\rm DC}$ may also suffer such uncertainties.

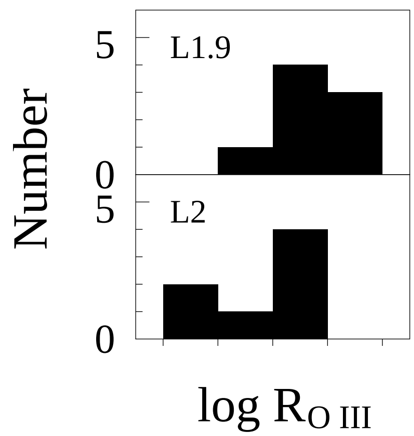

FIG. 13.— The frequency distributions of R_{OIII} for the L1.9s and the L2s.

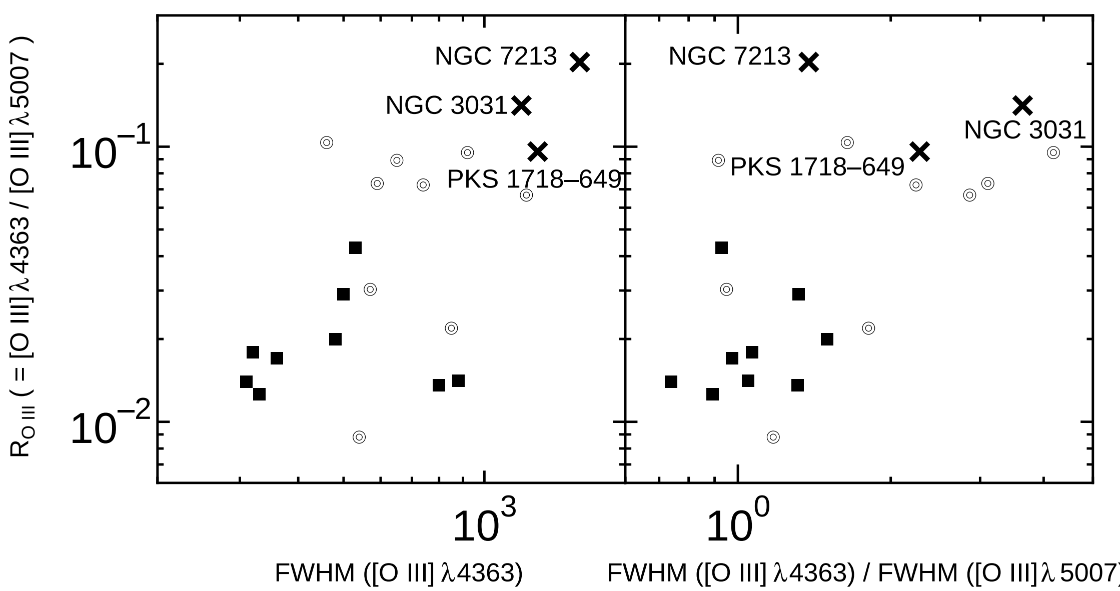

FIG. 14.— Same as Figure 9 but the sample of LINERs (NGC 3031, NGC 7213, and PKS 1718-649) are added. The crosses denote the LINERs.

Table 7
Observed values of $R_{\rm OIII}$ for LINERs

Object Name	$R_{\rm OIII}$	Reference[a]
	LINER with a broad component	
NGC 1052	0.0606	HFS93
	0.0353	HFS97
NGC 1275	0.0923	HFS93
NGC 3031	0.1884	HFS93
	0.0938	HFS96
NGC 3226	0.0901	HFS97
NGC 4278	0.1353	HFS97
NGC 4395	0.0312	HFS93
NGC 4579	0.0510	HFS97
NGC 7213	0.2030	FH84
	LINER without a broad component	
NGC 1167	0.0090	HFS93
NGC 1961	0.0750	HFS97
NGC 3504	0.0618	HFS93
NGC 4102	0.0300	HFS97
NGC 6500	0.0500	HFS97
NGC 7714	0.0121	HFS93
PKS 1718-649	0.0960	F85

[a] References for the data of $R_{\rm OIII}$. Each abbreviation means as follows; F85: Filippenko (1985); FH84: Filippenko & Halpern (1984); HFS93: Ho, Filippenko, & Sargent (1993); HFS96: Ho, Filippenko, & Sargent (1996); and HFS97: Ho, Filippenko, & Sargent (1997a).

In the sample, the emission-line width of [O III]λ4363 has been measured for three LINERs; NGC 3031 (Ho, Filippenko, & Sargent 1996), NGC 7213 (Filippenko & Halpern 1984), and PKS 1718-649 (Filippenko 1985). These data follow our dual component model; i.e., higher $R_{\rm OIII}$ objects show larger values of FWHM([O III]λ4363) and FWHM([O III]λ4363)/FWHM([O III]λ5007 (Figure 14).

These results seem to suggest that the [O III]λ4363 emitting regions are located at inner than the [O III]λ5007 emitting regions and that the [O III]λ4363 emission has an anisotropic property for LINERs, too. Further observations are needed to investigate this issue in detail.

5. SUMMARY

In this paper we proposed the idea that a large fraction of [O III]λ4363 originates in dense gas clouds obscured by the torus, which cause high values of $R_{\rm OIII}$ comparing to predictions of simple one-zone photoionization models. We have shown some observational properties of $R_{\rm OIII}$ which support our model.

- *The values of $R_{\rm OIII}$ of the NLS1s, the BLS1s, and the S1.5s are higher than those of the S2s.* This difference suggests a large fraction of [O III]λ4363 emission is hidden by the torus in S2s.
- *The higher-$R_{\rm OIII}$ objects show hotter MIR colors.* The hotter MIR colors are thought to be attributed to the hotter dusty grains located at the inner surface of the dusty tori, which can be seen if we see the torus from more face-on view. Therefore, this means that the higher $R_{\rm OIII}$ objects are seen from more face-on view toward dusty tori than the lower $R_{\rm OIII}$ objects.
- *The higher-$R_{\rm OIII}$ objects show stronger HINER emission.* Since a large fraction of HINER emission is thought to arise from dense gas clouds at the inner surface of the dusty tori (Murayama & Taniguchi 1998a, 1998b), this means that the higher $R_{\rm OIII}$ can be attributed to the significant flux contribution from such a high dense cloud as described by Pier & Voit (1995).
- *The S1s have wider FWHM([O III]λ4363) and FWHM([O III]λ4363)/FWHM([O III]λ5007) than the S2s.* This suggests that the [O III]λ4363 emitting regions are located inner than the [O III]λ5007 emitting regions and have an anisotropic property.
- *The higher-$R_{\rm OIII}$ objects show larger FWHM([O III]λ4363)/FWHM([O III]λ5007) ratios.* This also suggests that the [O III]λ4363 emitting regions are located inner than the [O III]λ5007 emitting regions.

As shown in section 3.4, there is too little information to discuss the kinematical and structural properties of the [O III]λ4363 emitting region because it is often difficult to observe this emission line accurately. Therefore further observations are needed to confirm this dual-component model. In particular, the spatial distribution of $R_{\rm OIII}$ should be investigated to judge the validity for this model. This dual-component model predicts that the higher $R_{\rm OIII}$ (~ 0.1) is seen only in nuclear region.

We would like to thank Gary Ferland for providing his code *Cloudy* to the public. We also thank the anonymous referee and Yasuhiro Shioya for some useful comments, and Shingo Nishiura for his kind assistance. YT would like to thank Rolf-Peter Kudritzki, Bob McLaren, and Dave Sanders at Institute for Astronomy, University of Hawaii for their warm hospitality. This research has made use of the NED (NASA extragalactic database) which is operated by the Jet Propulsion Laboratory, California Institute of Technology, under construct with the National Aeronautics and Space Administration. TM is supported by a Research Fellowship from the Japan Society for the Promotion of Science for Young Scientists. This work was financially supported in part by Grant-in-Aids for the Scientific Research (Nos. 10044052, and 10304013) of the Japanese Ministry of Education, Culture, Sports, and Science.

REFERENCES

Alonso-Herrero, A., Rieke, M. J., Rieke, G. H., & Shields, J. C. 2000, ApJ, 530, 688
Antonucci, R. R. J. 1993, ARA&A, 31, 473
Antonucci, R. R. J., & Miller, J. S. 1985, ApJ, 297, 621
Appenzeller, I., & Östreicher, R. 1988, AJ, 95, 45
Atwood, B., Baldwin, J. A., & Carswell, R. F. 1982, ApJ, 257, 559
Baldwin, J. A. 1975, ApJ, 201, L26
Baldwin, J. A., Phillips, M. M., & Terlevich, R. 1981, PASP, 93, 5
Barth, A. J., Filippenko, A. V., & Moran, E. C. 1999a, ApJ, 515, L61
Barth, A. J., Filippenko, A. V., & Moran, E. C. 1999b, ApJ, 525, 673
Barth, A. J., Reichert, G. A., Filippenko, A. V., Ho, L. C., Shields, J. C., Mushotzky, R. F., & Puchnarewicz, E. M. 1996, AJ, 112, 1829
Bergvall, N., Johansson, L., & Olofsson, K. 1986, A&A, 166, 92
Binette, L. 1985, A&A, 143, 334
Binette, L., Magris, C. G., Stasińska, G., & Bruzual, A. G. 1994, A&A, 292, 13
Boksenberg, A., Shortridge, K., Allen, D. A., Fosbury, R. A. E., Penston, M. V., & Savage, A. 1975, MNRAS, 173, 381
Boller, T., Brandt, W. N., & Fink, H. 1996, A&A, 305, 53
Boroson, T. A., & Green, R. F. 1992, ApJS, 80. 109
Brandt, W. N., & Boller, Th. 1999, ASP Conf. Ser. 175, in Structure and Kinematics of Quasar Broad Line Regions, ed. Gaskell, C. M. et al. (San Francisco: ASP), 265
Cardelli, J. A., Clayton, G. C., & Mathis, J. S. 1989, ApJ, 345,245
Cohen, R. D. 1983, ApJ, 273, 489
Cohen, R. D., & Osterbrock, D. E. 1981, ApJ, 243, 81
Costero, R., & Osterbrock, D. E. 1977, ApJ, 211, 675
Crenshaw, D. M., & Kraemer, S. B. 2000, ApJ, 532, L101
Crenshaw, D. M., Peterson, B. M., Korista, K. T., Wagner, R. M., & Aufdenberg, J. P. 1991, AJ, 101, 1202
Cruz-González, I., Carrasco, L., Serrano, A., Guichard, J., Dultzin-Hacyan, D., & Bisiacchi, G. F. 1994, ApJS, 94, 47
Cruz-González, I., Guichard, J., Serrano, A., & Carrasco, L. 1991, PASP, 103, 888
Dahari, O., & De Robertis, M. M. 1988, ApJS, 67, 249
Davidson, K. 1977, ApJ, 218, 20
Davidson, K., & Kinman, T. D. 1978, ApJ, 225, 776
De Robertis, M. M., & Osterbrock, D. E. 1984, ApJ, 286, 171 (DRO84)
De Robertis, M. M., & Osterbrock, D. E. 1986a, ApJ, 301, 98
De Robertis, M. M., & Osterbrock, D. E. 1986b, ApJ, 301, 727 (DRO86)
De Zotti, G., & Gaskell, C. M. 1985, A&A, 147, 1
Diaz, A. I., Prieto, M. A., & Wamsteker, W. 1988, A&A, 195, 53
Dopita, M. A., & Sutherland, R. S. 1995, ApJ, 455, 468
Durret, F., & Bergeron, J. 1988, A&AS, 75, 273
Efstathiou, A., & Rowan-Robinson, M. 1995, MNRAS, 273, 649
Espey, B. R. et al. 1994, ApJ, 434, 484
Evans, I., Koratkar, A., Allen, M., Dopita, M., & Tsvetanov, Z. 1999, ApJ, 521, 531
Fadda, D., Giuricin, G., Granato, G., & Vecchies, D. 1998, ApJ, 496, 117
Ferguson, J. W., Korista, K. T., Baldwin, J. A., & Ferland, G. J. 1997, ApJ, 487, 122
Ferland, G. J. 1996, Hazy: A Brief Introduction to Cloudy (Lexington; Univ. Kentucky Dept. Phys. Astron.)
Ferland, G. J., & Netzer, H. 1983, ApJ, 264, 105
Ferland, G. J., & Osterbrock, D. E. 1986, ApJ, 300, 658
Ferland, G. J., & Osterbrock, D. E. 1987, ApJ, 318, 145
Fillippenko, A. V. 1985, ApJ, 289, 475
Fillippenko, A. V., & Halpern, J. P. 1984, ApJ, 285, 458
Fillippenko, A. V., & Terlevich, R. 1992, ApJ, 397, L79
Fosbury, R. A. E., Mebold, U., Goss, W. M., & Dopita, M. A. 1978, MNRAS, 183, 549
Fosbury, R. A. E., & Sansom, A. E. 1983, MNRAS, 204, 1231
Giuricin, G., Mardirossian, F., & Mezzetti, M. 1995, ApJ, 446, 550
Glass, I. S. 1979, MNRAS, 186, 29
Glass, I. S. 1981, MNRAS, 197, 1067
Golev, V., Yankulova, I., Bonev, T., & Jockers, K. 1995, MNRAS, 273, 129
González Delgado, R. M., & Pérez, E. 1996, MNRAS, 281, 1105
Grevesse, N., & Anders. E. 1989, in AIP Conf. Proc. 183, Cosmic Abundance of Matter, ed. Waddington, C. J. (New York: AIP), 1
Grevesse, N., & Noels, A. 1993, in Origin & Evolution of the Elements, ed. Prantzos, N., Vangioni-Flam, E., & Casse, M. (Cambridge Univ. Press), 15
Heckman, T. M. 1980, A&A, 87, 152
Heckman, T. M. 1986, PASP, 98, 159
Heckman, T. M. 1995, ApJ, 446, 101
Heckman, T. M., & Balick, B. 1979, A&A, 79, 350
Heckman, T. M., Chambers, K. C., & Postman, M. 1992, ApJ, 391, 39
Heckman, T. M., Lebofsky, M. J., Rieke, G. H., & Van Breugel, W. 1983, ApJ, 272, 400
Ho, L. C., Filippenko, A. V., & Sargent, W. L. W. 1993, ApJ, 417, 63
Ho, L. C., Filippenko, A. V., & Sargent, W. L. W. 1996, ApJ, 462, 183
Ho, L. C., Filippenko, A. V., & Sargent, W. L. W. 1997a, ApJS, 112, 315
Ho, L. C., Filippenko, A. V., Sargent, W. L. W., & Peng, C. Y. 1997b, ApJS, 112, 391
Kaiser, M. E., Bradlew, L. D. II., Hutchings, J. B., Crenshaw, D. M., Gull, T. R., Kraemer, S. B., Nelson, C. H., Ruiz, J., & Weistrop, D. 2000, ApJ, 528, 260
Kemp, J. C., Rieke, G. H., Lebofsky, M. J., & Coyne, G. V. 1977, ApJ, 215, L107
Kollatschny, W., & Fricke, K. J. 1983, A&A, 125, 276
Korista, K. T., & Ferland, G. J. 1989, ApJ, 343, 678
Koski, A. T. 1978, ApJ, 223, 56
Koski, A. T., & Osterbrock, D. E. 1976, ApJ, 203, L49
Kraemer, S. B., Crenshaw, D. M., Filippenko, A. V., & Peterson, B. M. 1998, ApJ, 499, 719
Kraemer, S. B., Wu, C.-C., Crenshaw, D. M., & Harrington, J. P. 1994, ApJ, 435, 171
Kunth, D., & Sargent, W. L. W. 1979, A&A, 76, 50
Kwan, J., & Krolik, J. H. 1981, ApJ, 250, 478
Lípari, S., Tsvetanov, Z., & Macchetto F. 1993, ApJ, 405, 186
McLaren, R. A., Maza, J., McAlary, C. W., & McGonegal, R. J. 1983, ApJS, 52, 341
Moore, D., & Cohen, R. D. 1996, ApJ, 470, 301
Morris, S. L., & Ward, M. J. 1988, MNRAS, 230, 639
Moshir, M., et al. 1992, Explanatory Supplement to the *IRAS* Faint Source Survey (Version 2, JPL-D-10015 8/92; Pasadena: JPL)
Murayama, T. 1998, Doctor's thesis, Tohoku Univ.
Murayama, T., Mouri, H., & Taniguchi, Y. 2000, ApJ, 528, 179
Murayama, T., & Taniguchi, Y. 1998a, ApJ, 497, L9
Murayama, T., & Taniguchi, Y. 1998b, ApJ, 503, L115
Murayama, T., Taniguchi, Y., & Iwasawa, K. 1998, AJ, 115, 460
Nagao, T., Murayama, T., & Taniguchi, Y. 2000a, ApJ, 545, in press (astro-ph/0008006)
Nagao, T., Murayama, T., Taniguchi, Y., & Yoshida, M. 2000b, AJ, 119, 620
Nagao, T., Taniguchi, Y., & Murayama, T. 2000c, AJ, 119, 2605
Nelson, C. H., Weistrop, D., Hutching, J.B., Crenshaw, D. M., Gull, T. R., Kaiser, M. E., Kraemer, S. B., & Lindler, D. 2000, ApJ, 531, 257
O'Connell, R. W., & Kingham, K. A. 1978, PASP, 90, 244
Osterbrock, D. E. 1977, ApJ, 215, 733
Osterbrock, D. E. 1981, ApJ, 246, 696
Osterbrock, D. E. 1985, PASP, 97, 25
Osterbrock, D. E. 1993, ApJ, 404, 551
Osterbrock, D. E., Koski, A. T., & Phillips, M. M. 1976, ApJ, 206, 898
Osterbrock, D. E., & Pogge, R. W. 1985, ApJ, 297, 166
Pelat, D., Fosbury R. A. E., & Alloin, D. 1981, MNRAS, 195, 787
Phillips, M. M. 1978, ApJ, 226, 736
Phillips, M. M., Charles, P. A., & Baldwin, J. A. 1983, ApJ, 266, 485
Phillips, M. M., & Frogel, J. A. 1980, ApJ, 235, 761
Pier, E. A., & Krolik, J. H. 1992, ApJ, 401, 99
Pier, E. A., & Voit, G. M. 1995, ApJ, 450, 628
Press, W. H., Teukolsky, S. A., Vetterling, W. T., & Flannery, B. P. 1988, Numerical Recipes in C (Cambridge University Press)
Reynolds, C. S., Ward, M. J., Fabian, A. C., & Celotti, A. 1997, MNRAS, 291, 403
Rieke, G. H. 1978, ApJ, 226, 550
Rieke, G. H., & Low, F. J. 1972, ApJ, 176, L95
Rodríguez-Ardia, A., Pastoriza, M. G., & Donzelli, C. J. 2000, ApJS, 126, 63
Rudy, R. J., Levan, P. D., & Rodríguez-Espinosa, J. M. 1982, AJ, 87, 598
Schmitt, H. R. 1998, ApJ, 506. 647
Schmitt, H. R., & Kinney, A. L. 1996, ApJ, 463, 498
Shuder, J. M. 1980, ApJ, 240, 32
Shuder, J. M. 1981, ApJ, 244, 12
Shuder, J. M., & Osterbrock, D. E. 1981, ApJ, 250, 55
Stauffer, J., Schild, R., & Keel, W. 1983, ApJ, 270, 465
Stein, W. A., & Weedman, D. W. 1976, ApJ, 205, 44
Stephens, S. A. 1989, AJ, 97, 10
Sulentic, J. W., Zwitter, T., Marziani, P., & Dultzin-Hacyan, D. 2000, ApJ, 536, L5
Taniguchi, Y., Shioya, Y., & Murayama, T. 2000, AJ, 120, 1265

Terlevich, R., Melnick, J., Masegosa, J., Moles, M., & Copetti, M. V. F. 1991, A&AS, 91, 285
Ulrich, M. -H., & Péquignot, D. 1980, ApJ, 238, 45
Vaughan, S., Reeves, J., Warwick, R., & Edelson, R. 1999, MNRAS, 309, 113
Véron-Cetty, M. -P., & Véron, P. 1998, ESO Sci. Rept. No.18 (European Southern Observatory)
Viegas-Aldrovandi, S. M., & Gruenwald, R. B. 1988, ApJ, 324, 683
Ward, M., Penston, M. V., Blades, J. C., & Turtle, A. J. 1980, MNRAS, 193, 563
Wilson, A. S., Binette, L., & Storchi-Bergmann, T. 1997, ApJ, 482, L131
Winkler, H. 1992, MNRAS, 257, 677
Yee, H. K. C. 1980, ApJ, 241, 894
Zamorano, J., Gallego, J., Rego, M., Vitores, A. G., & Gonzalez-Riestra, R. 1992, AJ, 104, 1000

Table 1. The Properties of the Objects in Our Sample

Name	Another Name	Redshift	$R_{\rm OIII}$[a]	References[b]	$F_\nu(3.5\mu{\rm m})$ (Jy)	References[c]	$F_\nu(12\mu{\rm m})$[d] (Jy)	$F_\nu(25\mu{\rm m})$[d] (Jy)	$F_\nu(60\mu{\rm m})$[d] (Jy)
NLS1									
NGC 4748	MCG -2-33-34	0.0146	0.0492	RAPD00	···	···	0.1708	0.3705	1.163
Mrk 42	···	0.0240	0.1339	C91, K78, OP85	···	···	< 0.0987	< 0.1394	0.3172
Mrk 291	···	0.0352	0.1031	O77	···	···	< 0.0662	< 0.0884	0.3368
Mrk 335	PG 0003+199	0.0258	0.0699	O77, P78	0.0982	M83	0.3021	0.3777	0.3433
Mrk 359	UGC 1032	0.0174	0.0735	DK78, OP85	···	···	0.1192	0.4376	1.132
Mrk 493	UGC 10120	0.0319	0.4568	C91, OP85	0.0155	RLRE82	0.0881	0.1918	0.6937
Mrk 504	PG 1659+294	0.0359	0.0308	O77	0.0093	SW76	···	···	···
Mrk 507	···	0.0559	0.0593	K78	···	···	0.0531	0.1042	0.5445
Mrk 766	NGC 4253	0.0129	0.0294	CG94, OP85	0.0543	RLRE82	0.3855	1.295	4.026
Mrk 783	···	0.0672	0.0895	OP85	···	···	< 0.1005	< 0.1992	0.3096
Mrk 957	5C 3.100	0.0711	0.0952	K78	···	···	< 0.1882	0.245	2.095
Mrk 1126	NGC 7450	0.0106	0.1163	OP85	···	···	···	···	···
Mrk 1239	···	0.0199	0.0892	C91, CG94, OP85, RAPD00	0.157	RLRE82	0.650	1.141	1.335
1E 1031+5822	···	0.248	0.0683	S89	···	···	···	···	···
1E 1205+4657	···	0.102	0.3646	S89	···	···	···	···	···
1E 12287+123	···	0.116	0.5395	S89	···	···	···	···	···
2E 1226+1336	···	0.150	0.0312	S89	···	···	···	···	···
I Zw 1	UGC 545	0.0611	0.0761	O77, P78	0.111	SW76	0.5118	1.211	2.243
H 34.06	IRAS F06083-5606	0.0318	0.1023	RAPD00	···	···	< 0.0614	0.0882	0.2373
H 1934-063	IRAS 19348-0619	0.0106	0.0437	RAPD00	···	···	0.4963	1.064	2.808
HE 1029-1831	IRAS 10295-1831	0.0403	0.0980	RAPD00	···	···	0.1391	0.4108	2.545
IRAS 15091-2107	···	0.0446	0.0500	W92	···	···	0.2304	0.4986	1.521
J 13.12	···	0.0120	0.3101	RAPD00	···	···	···	···	···
Kaz 320	···	0.0345	0.0595	Z92	···	···	···	···	···
MS 01119-0132	···	0.120	0.1188	S89	···	···	···	···	···
MS 01442-0055	···	0.080	0.0207	S89	···	···	···	···	···
BLS1									
NGC 4235	···	0.0080	0.2837	MW88	0.0258	RLRE82	< 0.1259	< 0.1566	0.3164
Mrk 10	UGC 4013	0.0293	0.0247	O77	0.0134	SW76	0.1396	0.2206	0.813
Mrk 40	Arp 151	0.0211	0.1667	O77	···	···	···	···	···
Mrk 69	···	0.0760	0.0837	O77	···	···	···	···	···
Mrk 79	UGC 3973	0.0222	0.0457	C83, O77	0.0487	SW76	0.3062	0.7625	1.503
Mrk 106	···	0.1235	0.0310	O77	···	···	···	···	···
Mrk 124	···	0.0563	0.0730	O77, P78	0.0307	SW76	0.1188	0.2664	0.6831
Mrk 141	···	0.0417	0.0816	O77	0.011	R78	0.1279	0.1624	0.7408
Mrk 142	PG 1022+519	0.0449	0.0680	O77	···	···	···	···	···
Mrk 236	···	0.0520	0.0804	O77	···	···	< 0.0636	< 0.0963	0.1733
Mrk 279	UGC 8823	0.0294	0.0670	C83, O77	0.032	R78	< 0.205	< 0.3328	1.255
Mrk 304	II Zw 175, PG 2214+139	0.0658	0.1061	O77	0.0337	SW76	···	···	···
Mrk 374	···	0.0435	0.0738	O77, P78	0.0147	SW76	0.1123	0.194	0.2658
Mrk 382	···	0.0338	0.0322	O77	···	···	< 0.1469	< 0.2431	0.2154
Mrk 541	···	0.0394	0.2217	O77	0.0123	M83	< 0.140	< 0.180	0.3504
Mrk 590	NGC 863	0.0264	0.2000	O77	···	···	0.1917	0.2214	0.4893
Mrk 618	···	0.0356	0.0410	P78	···	···	0.3365	0.7884	2.706
Mrk 704	···	0.0292	0.0726	C83	0.0666	RLRE82	0.3543	0.5324	0.3636
Mrk 876	PG 1613+658	0.1290	0.2717	S89	···	···	< 0.0972	0.2369	0.5973
Mrk 975	UGC 774	0.0496	0.0303	C83	···	···	0.2488	0.3718	0.8001

TABLE 1. (continued)

Name	Another Name	Redshift	$R_{\rm OIII}$[a]	References[b]	$F_\nu(3.5\mu m)$ (Jy)	References[c]	$F_\nu(12\mu m)$[d] (Jy)	$F_\nu(25\mu m)$[d] (Jy)	$F_\nu(60\mu m)$[d] (Jy)
1E 0514-0030	···	0.292	0.4949	S89	···	···	···	···	···
1H 1927-516	···	0.0403	0.0792	RAPD00	···	···	···	···	···
1H 2107-097	···	0.0268	0.1696	RAPD00	···	···	···	···	···
2E 0150-1015	···	0.361	0.0341	S89	···	···	···	···	···
2E 0237+3953	···	0.528	0.0757	S89	···	···	···	···	···
2E 1401+0952	···	0.441	0.0565	S89	···	···	···	···	···
2E 1556+2725	PGC 56527	0.0904	0.0884	S89	···	···	···	···	···
2E 1847+3329	···	0.509	0.0649	S89	···	···	···	···	···
3C 263	···	0.646	0.0515	P78	···	···	···	···	···
3C 382	···	0.0579	0.1600	O77	0.036	H83	···	···	···
III Zw 2	···	0.0898	0.0273	O77	0.036	R78	···	···	···
A 08.12	···	0.0293	0.0759	RAPD00	···	···	···	···	···
Arp 102 B	···	0.0242	0.0571	SSK83	···	···	···	···	···
B2 1425+26	PG 1425+267	0.3660	0.0417	P78	···	···	···	···	···
B2 1512+37	PG 1512+370	0.3707	0.0393	P78	···	···	···	···	···
C 16.16	···	0.0795	0.0588	RAPD00	···	···	···	···	···
ESO 438-G09	···	0.0245	0.0541	KF83	···	···	< 0.3208	0.6241	3.144
ESO 578-G09	···	0.0349	0.0898	RAPD00	···	···	···	···	···
F 10.01	···	0.0784	0.0391	RAPD00	···	···	···	···	···
Fairall 9	ESO 113-IG45	0.0470	0.1200	W92	0.125	M83	···	···	···
Fairall 1116	Tololo 0349-406	0.0582	0.0900	W92	···	···	< 0.0981	0.1313	0.1577
Fairall 1146	···	0.0316	0.0436	RAPD00	···	···	···	···	···
H 34.03	IRAS F05561-5357	0.0967	0.1287	RAPD00	···	···	0.0796	0.1694	0.4799
J 10.09	IRAS F12312-2047	0.0230	0.1565	RAPD00	···	···	< 0.1252	< 0.1873	0.3816
M 02.30	IRAS F10306-2651	0.0688	0.1875	RAPD00	···	···	< 0.0864	< 0.105	0.2557
MC 1104+167	4C 16.30	0.632	0.0941	P78	···	···	···	···	···
MS 02255+3121	···	0.058	0.1270	S89	···	···	···	···	···
MS 07451+5545	···	0.174	0.0337	S89	···	···	···	···	···
MS 08451+3751	···	0.307	0.1198	S89	···	···	···	···	···
MS 08495+0805	···	0.062	0.0395	S89	···	···	···	···	···
MS 11397+1040	···	0.150	0.0215	S89	···	···	···	···	···
MS 15251+1551	···	0.230	0.0405	S89	···	···	···	···	···
MS 22152-0347	···	0.242	0.0329	S89	···	···	···	···	···
PKS 1417-19	···	0.120	0.1039	RAPD00	···	···	···	···	···
Tololo 20	···	0.030	0.0924	MW88	···	···	···	···	···
Ton 1542	Mrk 771, PG 1229+204	0.0640	0.1167	P78	0.0194	RLRE82	···	···	···
S1.5									
NGC 985	···	0.0431	0.1351	CG94	···	···	0.2075	0.5232	1.381
NGC 1019	···	0.0242	0.8387	PCB83	···	···	< 0.1381	< 0.1454	0.3549
NGC 1566	···	0.0050	0.1600	W92	0.0519	G81	0.831	1.219	14.71
NGC 3227	···	0.0039	0.0314	C83, O77	0.0783	M83	0.6671	1.764	7.825
NGC 3516	···	0.0088	0.0381	O77, P78, UP80	···	···	0.4258	0.8937	1.758
NGC 3783	···	0.0097	0.0500	W92	0.0509	M83	0.8394	2.492	3.257
NGC 4151	···	0.0033	0.0219	B75	0.314	K77	···	···	···
NGC 5548	···	0.0172	0.1025	C83, O77	0.0986	M83	0.4006	0.769	1.073
NGC 6814	···	0.0052	0.0715	MW88	0.0329	M83	< 0.4896	0.5986	5.517
NGC 6860	···	0.0149	0.0672	LTM93	···	···	0.2397	0.3321	0.9538
NGC 7469	···	0.0163	0.0336	C83, O77, P78	0.117	G81	1.348	5.789	25.87
Mrk 6	IC 450	0.0185	0.0179	C83, K78	0.046	R78	0.2239	0.6866	1.183
Mrk 9	···	0.0399	0.0667	P78	0.0487	SW76	0.2147	0.439	0.7676

TABLE 1. (continued)

Name	Another Name	Redshift	$R_{\rm OIII}$[a]	References[b]	$F_\nu(3.5\mu m)$ (Jy)	References[c]	$F_\nu(12\mu m)$[d] (Jy)	$F_\nu(25\mu m)$[d] (Jy)	$F_\nu(60\mu m)$[d] (Jy)
Mrk 110	PG 0921+525	0.0353	0.0463	O77	0.0097	SW76	···	···	···
Mrk 290	PG 1534+580	0.0296	0.0429	O77	0.0212	SW76	< 0.1065	< 0.1441	0.1708
Mrk 315	···	0.0389	0.0652	K78	0.017	R78	< 0.2274	0.3318	1.464
Mrk 372	IC 1854	0.0310	0.0266	K78	0.0102	SW76	< 0.128	0.1675	0.303
Mrk 506	···	0.0430	0.0402	C83, O77	0.0128	SW76	···	···	···
Mrk 609	···	0.0341	0.1486	CG94	···	···	···	···	···
Mrk 699	III Zw 77	0.0342	0.1035	FO87, KS79, O81, OK78	···	···	< 0.138	< 0.0851	0.2453
Mrk 817	UGC 1501+106	0.0315	0.0425	C83	0.0601	RLRE82	0.3355	1.175	2.118
Mrk 841	PG 1501+106	0.0362	0.0119	C83	0.0409	RLRE82	0.1924	0.4726	0.4593
Mrk 864	···	0.0719	0.0310	S89	···	···	< 0.1241	0.1348	0.2859
Mrk 926	MCG -2-58-22	0.0473	0.0795	C83, DB88, MW88	0.0473	RLRE82	···	···	···
Mrk 1320	···	0.1030	1.3917	MW88	···	···	< 0.0980	< 0.1239	0.2182
Mrk 1393	···	0.0544	0.0298	MW88	···	···	···	···	···
1E 0057+3110	···	0.287	0.0765	S89	···	···	···	···	···
1E 1011+0329	···	0.313	0.0635	S89	···	···	···	···	···
1H 1142-178	IRAS F11431-1810	0.0329	0.0306	W92, RAPD00	···	···	< 0.1163	< 0.1199	0.2285
2E 0844+3743	···	0.451	0.1353	S89	···	···	···	···	···
2E 1008+3452	···	0.140	0.0130	S89	···	···	···	···	···
2E 1227+1403	···	0.100	0.2549	S89	···	···	···	···	···
2E 1615+0611	IRAS 16154+0611	0.0379	0.0562	MW88	···	···	< 0.2925	< 0.1328	0.8438
3C 120	···	0.0330	0.0864	DB88, O77	0.070	RL72	0.2861	0.6353	1.283
3C 227	···	0.0862	0.0802	O77	···	···	···	···	···
3C 281	···	0.602	0.1080	P78	···	···	···	···	···
3C 380	···	0.692	0.0714	P78	···	···	···	···	···
3C 390.3	···	0.0561	0.1212	O77	0.016	H83	0.1277	0.2873	0.2037
3C 445	IRAS F22212-0221	0.0562	0.0610	MW88, O77	···	···	0.2076	0.2637	0.3061
4C 61.20	···	0.422	0.0480	P78	···	···	···	···	···
II Zw 1	···	0.0543	0.0258	O77	···	···	< 0.1472	0.2713	1.455
B3 0754+394	IRAS F07546+3928	0.096	0.0297	S89	···	···	< 0.1395	0.2756	0.1729
ESO 362-G18	MCG -5-13-17	0.0126	0.0619	RAPD00, W92	···	···	0.2238	0.5699	1.396
Fairall 51	ESO 140-G43	0.0142	0.0400	W92	0.118	G81	< 0.4671	1.035	1.844
MCG -6-30-15	ESO 383-G35	0.0077	0.0778	MW88, R97	0.0877	M83	0.3803	0.8088	1.087
MCG 8-11-11	UGC 3374	0.0205	0.0223	C83	0.0874	M83	0.6394	1.948	3.005
MR 2251-178	···	0.068	0.1300	F85	0.0182	M83	< 0.1521	< 0.2128	0.312
MS 01363+0606	···	0.450	0.1155	S89	···	···	···	···	···
MS 04124-0802	IRAS 04124-0803	0.0379	0.0190	S89	···	···	0.1891	0.5205	0.6335
MS 13285+3135	···	0.241	0.1071	S89	···	···	···	···	···
PKS 0518-45	Pictor A	0.0351	0.0960	F85	0.0233	G79	···	···	···
PKS 2344+09	···	0.677	0.0391	P78	···	···	···	···	···
SBS 1701+610	···	0.164	0.0548	S89	···	···	···	···	···
Ton 236	···	0.450	0.0384	S89	···	···	···	···	···
S1.8									
Mrk 334	UGC 6	0.0220	0.0726	CG94	···	···	0.2257	1.048	4.345
Mrk 744	NGC 3786	0.0089	0.2167	CG94	···	···	···	···	···
Mrk 1218	NGC 2622	0.0286	0.0547	CG94	···	···	< 0.1337	< 0.3364	0.4283
MS 04494-1823	···	0.3387	0.0428	S89	···	···	···	···	···
S1.9									
NGC 424	Tololo 0109-383	0.0117	0.0499	FS83, MTI98, T91	···	···	1.101	1.739	1.796

Table 1. (continued)

Name	Another Name	Redshift	$R_{\rm OIII}$[a]	References[b]	$F_\nu(3.5\mu$m) (Jy)	References[c]	$F_\nu(12\mu$m)[d] (Jy)	$F_\nu(25\mu$m)[d] (Jy)	$F_\nu(60\mu$m)[d] (Jy)
NGC 513	Akn 41	0.0195	0.2674	CG94	···	···	0.1665	0.2769	1.935
NGC 2110	···	0.0076	0.0429	CG94, S80	0.0822	G81	0.3488	0.8397	4.129
NGC 2992	···	0.0077	0.0200	S80, W80	0.0724	M83	···	···	···
NGC 3982	···	0.0037	0.0016	PCB83	···	···	0.5073	0.8335	6.567
NGC 4507	···	0.0118	0.0283	PCB83	0.073	G81	0.4566	1.387	4.310
NGC 5252	···	0.0231	0.0759	CG94	···	···	···	···	···
NGC 5674	···	0.0249	0.1046	CG94	···	···	0.1441	0.281	1.444
NGC 5728	···	0.0093	0.0288	PCB83	···	···	0.2434	0.8817	8.163
NGC 6890	···	0.0081	0.0303	PCB83	···	···	0.3422	0.6541	3.855
NGC 7314	···	0.0047	0.0215	MW88	···	···	0.2679	0.5788	3.736
Mrk 1388	···	0.0213	0.0514	O85	···	···	$<$ 0.1536	0.2309	0.1744
3C 219	···	0.1744	0.0570	CO81	···	···	···	···	···
IC 5135	NGC 7130	0.0162	0.0256	PCB83	···	···	0.5882	2.117	16.48
PKS 2048-57	IC 5063	0.0113	0.0200	PCB83	···	···	1.067	3.910	5.337
Tololo 1351-375	Tololo 113	0.0520	0.0229	MW88	···	···	0.1063	0.3162	0.4524
$S2_{\rm NIR-BLR}$									
NGC 5506	···	0.0062	0.0126	MW88, S80	0.255	M83	1.282	3.638	8.409
Mrk 176	UGC 6527	0.0274	0.0139	K78	0.0255	SW76	0.1702	0.2421	0.6937
3C 184.1	···	0.1182	0.0262	K78	···	···	···	···	···
3C 223	···	0.1368	0.0230	CO81	···	···	···	···	···
ESO434-G40	MCG -5-23-16	0.0083	0.0700	W92	0.1068	M83	···	···	···
$S2_{\rm HBLR}$									
NGC 788	···	0.0136	0.0372	CG94	···	···	0.1869	$<$ 0.5148	0.5105
NGC 1068	Messier 77	0.0038	0.0129	K78	1.70	RL72	39.70	85.04	176.2
NGC 4388	···	0.0084	0.0245	CG94, S80	···	···	0.9964	3.463	10.24
NGC 7674	Mrk 533	0.0291	0.0088	K94, SO81	···	···	0.6724	1.896	5.588
Mrk 3	UGC 3426	0.0135	0.0141	K78	0.036	R78	0.7125	2.896	3.770
Mrk 348	NGC 262	0.0150	0.0170	K78	0.0369	SW76	0.308	0.8347	1.290
Mrk 477	I Zw 92	0.0378	0.0291	K94, KS79, OK78, SO81	···	···	0.1263	0.5093	1.313
Mrk 1210	UGC 4203	0.0135	0.0410	T91	···	···	0.4965	2.075	1.892
$S2^-$									
NGC 1229	···	0.0363	0.0348	PCB83	···	···	0.1466	0.6312	1.548
NGC 1358	···	0.0134	0.0625	PCB83	···	···	$<$ 0.0829	$<$ 0.1236	0.3781
NGC 1386	···	0.0029	0.0382	PCB83	0.046	PF80	0.4927	1.433	5.396
NGC 1410	III Zw 55, UGC 2821	0.0253	0.0206	K78	0.008	R78	···	···	···
NGC 3081	···	0.0080	0.0150	PCB83	···	···	···	···	···
NGC 3281	···	0.0107	0.0293	DB88, PCB83	···	···	0.8896	2.633	6.861
NGC 3393	···	0.0125	0.0099	DPW88	···	···	0.131	0.7528	2.251
NGC 5135	···	0.0137	0.0166	PCB83	···	···	0.638	2.401	16.91
NGC 5643	···	0.0040	0.0193	PCB83	···	···	1.098	3.647	19.49
NGC 6300	···	0.0037	0.0379	PCB83	···	···	0.9268	2.272	14.65
NGC 7582	···	0.0053	0.0175	CG94, W80	0.160	G81	1.620	6.436	49.10
NGC 7682	···	0.0171	0.0117	CG94	···	···	···	···	···
Mrk 1	NGC 449	0.0159	0.0136	K78	0.011	R78	$<$ 1.887	0.8648	2.531
Mrk 34	···	0.0505	0.0110	K78	0.010	R78	0.0684	0.464	0.8092
Mrk 78	···	0.0372	0.0075	K78	0.011	R78	0.1278	0.5546	1.110

Table 1. (continued)

Name	Another Name	Redshift	$R_{\rm OIII}$[a]	References[b]	$F_\nu(3.5\mu$m) (Jy)	References[c]	$F_\nu(12\mu$m)[d] (Jy)	$F_\nu(25\mu$m)[d] (Jy)	$F_\nu(60\mu$m)[d] (Jy)
Mrk 198	···	0.0240	0.0192	K78	0.009	R78	< 0.1209	0.1364	0.8236
Mrk 268	···	0.0399	0.0417	K78	0.007	R78	0.1083	0.2798	1.381
Mrk 270	NGC 5283	0.0090	0.0292	K78	0.007	R78	···	···	···
Mrk 273	UGC 8696	0.0378	0.0257	K78	0.019	R78	0.2352	2.282	21.74
Mrk 461	UGC 8718	0.0162	0.1150	CG94	···	···	< 0.0989	0.1242	0.3749
Mrk 573	UGC 1214	0.0173	0.0179	K78	···	···	< 0.250	< 0.932	1.088
Mrk 607	NGC 1320	0.0091	0.0294	DRO86	···	···	0.3303	1.065	2.152
Mrk 612	···	0.0203	0.0150	SO81	···	···	0.128	0.2675	1.159
Mrk 622	UGC 4229	0.0232	0.0040	SO81	···	···	< 0.1875	0.4051	1.281
Mrk 686	NGC 5695	0.0141	0.1577	CG94	···	···	< 0.1053	0.1288	0.5655
3C 33	···	0.0592	0.0203	K78	···	···	···	···	···
3C 98	···	0.0305	0.0246	CO77	···	···	···	···	···
3C 99	···	0.426	0.0150	CO81	···	···	···	···	···
3C 192	···	0.0598	0.0311	CO77	···	···	···	···	···
3C 223.1	···	0.1075	0.0200	CO81	···	···	···	···	···
3C 317	UGC 9799	0.0342	0.1100	CO81	···	···	···	···	···
3C 327	IRAS 15599+0206	0.1048	0.0156	CO77, OK78	···	···	0.0918	0.3194	0.5993
3C 433	···	0.1016	0.0307	K78	···	···	···	···	···
3C 452	···	0.0811	0.0191	K78	···	···	···	···	···
4C 39.72	···	0.2061	0.0320	CO81	···	···	···	···	···
Akn 79	UGC 1757	0.0175	0.1327	CG94	···	···	···	···	···
Akn 347	NGC 4074	0.022	0.0200	SO81	···	···	···	···	···
ESO 306-G25	Tololo 0544-395	0.025	0.0222	T91	···	···	< 0.0867	0.1144	0.1968
ESO 428-G14	···	0.0054	0.0180	BJO86	···	···	···	···	···
ESO 540-G14	···	0.0055	0.0392	CG94	···	···	< 0.133	< 0.0989	0.2797
IC 1515	···	0.0222	0.0432	PCB83	···	···	< 0.1528	< 0.2345	0.5658
UGC 6100	···	0.0293	0.0234	CG94	···	···	0.1453	0.2018	0.5743
UM 16	···	0.0579	0.0140	SO81, T91	···	···	···	···	···
UM 82	···	0.051	0.0127	T91	···	···	···	···	···
UM 625	···	0.025	0.0212	T91	···	···	< 0.133	< 0.1211	0.3209

[a] $R_{\rm OIII}$ is the emission-line ratio of [O III]λ4363/[O III]λ5007.

[b] References for the data of $R_{\rm OIII}$. Each abbreviation means as follows; B75: Boksenberg et al. (1975); BJO86: Bergvall, Johansson, & Olofsson (1986); C83: Cohen (1983); C91: Crenshaw et al. (1991); CG94: Cruz-Gonzárez et al. (1994); CO77: Costero & Osterbrock (1977); CO81: Cohen & Osterbrock (1981); DB88: Durret & Bergeron (1988); DRO86: De Robertis & Osterbrock (1986a); DK78: Davidson & Kinman (1978); DPW88: Diaz, Prieto, & Wamsteker (1988); F85: Filippenko (1985); FO87: Ferland & Osterbrock (1987); FS83: Fosbury & Sansom (1983); K78: Koski (1978); K94: Kraemer et al. (1994); KF83: Kollatshny & Fricke (1983); KS79: Kunth & Sargent (1979); LTM93: Lípari, Tsvetanov, & Macchetto (1993); MW88: Morris & Ward (1992); MTI98: Murayama, Taniguchi, & Iwasawa (1998); O77: Ostrbrock (1977); O81: Osterbrock (1981); O85: Osterbrock (1985); OK78: O'connell & Kingham (1978); OP85: Osterbrock & Pogge (1985); P78: Phillips (1978); PCB83: Phillips, Charles, & Baldwin (1983); R97: Reynolds et al. (1997); RAPD00: Rodríguez-Ardia, Pastoriza, & Donzelli (2000); S80: Shuder (1980); S89: Stephens (1989); SO81: Shuder & Osterbrock (1981); SSK83: Stauffer, Schild, & Keel (1983); T91: Terlevich et al. (1991); UP80: Ulrich & Péquignot (1980); W80: Ward et al. (1980); W92: Winkler (1992); and Z92: Zamorano et al. (1992)

[c] References for the data of $F_\nu(3.5\mu$m). Each abbreviation means as follows; G79: Glass (1979); G81: Glass (1981); H83: Heckman et al. (1983); K77: Kemp et al. (1977); M83: McLaren et al. (1983); PF80: Phillips & Frogel (1980); R78: Rieke (1978); RL72: Rieke & Low (1972); RLRE82: Rudy, Leven, & Rodriguez-Espinosa (1982); and SW76: Stein & Weedman (1976).

[d] Data taken from Moshir et al. (1992)